The Aerospike Nozzle:

An Investigation into a Single Stage to Orbate (SSTO) Rocket Engine

High Altitude Student Platform (HASP)

Summer 2007

By: Theodore Bounds & John Dykes

Group Members: Theodore Bounds, John Dykes, Jeff Kornuta, Henry Hardee, Matt Hoenscheutz, Edward Scheuermann, & Ian Walsdorf

Dr. S. M. Guo & Dr. T. G. Guzik

Abstract

In the aerospace industry, there is a growing demand for a space craft that can safely and effectively launch payloads into space while being economically feasible. To achieve this, various rocket engine designs have been explored. One that has significant potential is termed the aerospike nozzle rocket engine. This is because the aerospike nozzle allows the exsausting propellant to expand externally rather than internally as is the case for the traditional Converging-Diverging type rocket nozzle. Aerodynamic theory predicts that the aerospike will be able to compensate for the changes in atmospheric and, thus, allow it to achieve a greater efficiency at a wider range of altitudes than that of the C-D nozzle. This meanse that the aerospike nozzle could greatly reduce the specific fuel consumtpion of a space craft while maintaining a sufficient thrust needed to propel the craft into space. This experiment is an investigation into that claim and directly compares the performance of a traditional C-D nozzle to that of the aerospike nozzle. Coefficients of thrusts are compared also to a third source of comparison as a FLUENT® Analysis was performed in an attempt to valid the data that was obtained experimentally.

Table of Contents

Table of Figures

Introduction

The demands of a growing orbital communications industry will soon outstrip the capabilities of our current fleet for launching payloads into space. The Ares V launch vehicle will soon replace the aging Space shuttle in this function, but will not provide the low-cost access to space demanded by the modern world. For these reasons, serious considerations have been made by several worldwide aerospace organizations into the feasibility of a reusable single-stage-to-orbit (SSTO) craft capable of bringing payloads into space with an efficiency and regularity approaching that of an airline [1].

A requirement of these SSTO craft is that they be able to reach orbit without jettisoning any hardware in the process. As a consequence, the chosen form(s) of propulsion must have low mass and be efficient, yet powerful in all stages of flight encountered by the craft. One potential solution, proposed by many, is the use of the aerospike rocket (AS) nozzle, the promise of which lies in its inherent ability to compensate for altitude and provide adequate thrust consistently and efficiently for all altitudes encountered during the flight.

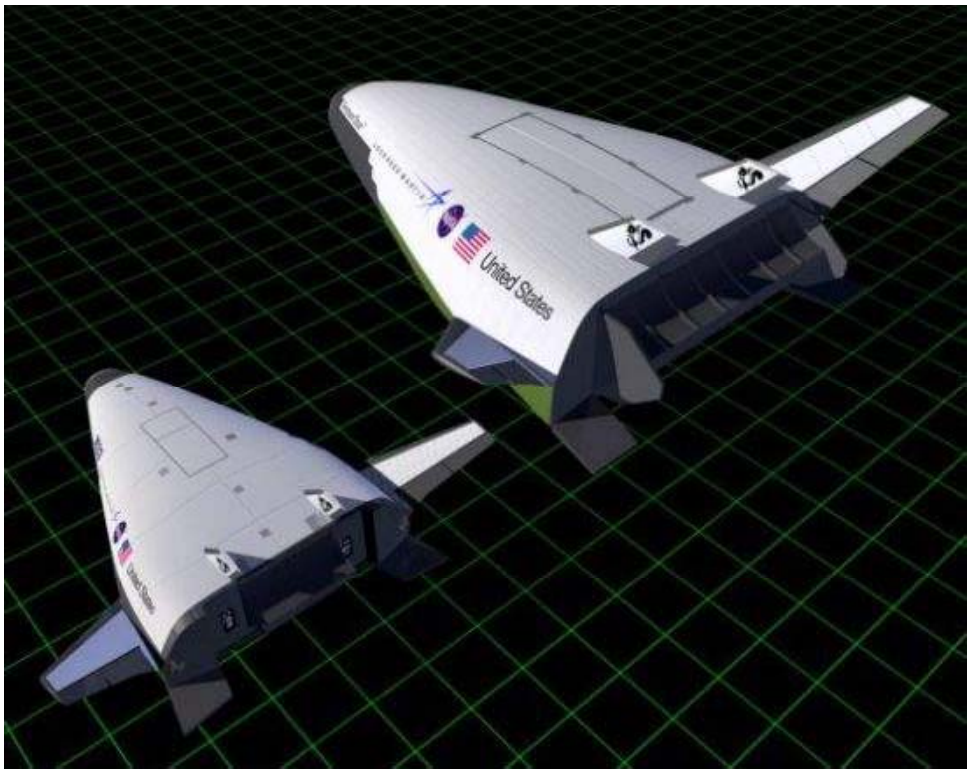

Figure 1: An example of a SSTO craft (Lockheed Martin's X-33 project) [2]

Currently, the converging-diverging (C-D) bell-shaped nozzle serves as the sole workhorse for launching payloads into space. In this function, C-D nozzle engines are powerful, reliable, and mature in design, but also tend to be inefficient in overall operation [2]. In C-D rockets, the hot, high-pressure, subsonic gas from the thrust chamber is converged into the smaller throat area where it is accelerated to the speed of sound (Mach 1). From there, the gas flows into a divergent section where it is expanded and accelerated to supersonic speeds [3]. This high-velocity exhaust, in addition to the pressure force on the nozzle walls, is what generates the thrust force [4].

The area ratio (exit area/throat area) of a C-D nozzle is chosen based on a specific altitude and backpressure deemed most critical for the operation of the craft. At the ideal altitude, the exhaust leaving the exit plane of the nozzle has been expanded to the atmospheric backpressure, creating a column-shaped plume that provides maximum thrust and efficiency.

The penalty for operating a C-D nozzle outside of the ideal backpressure can be significant. In the case where the exhaust exit pressure is higher than the atmospheric pressure, the exhaust is referred to as being *underexpanded*. This is typified by an exhaust plume that expands outward behind the exit and by the formation of expansion waves angled off the rear of the nozzle. When this occurs, valuable expansion work and acceleration of the exhaust gas is done outside of the nozzle and, as such, is not "felt" as thrust by the nozzle [2]. Also detrimental to the performance is the case where the exhaust is *overexpanded* in the nozzle and the exit pressure is less than the ambient pressure. This is characterized by a "pinched" exhaust plume and by shock wave formation either as oblique shocks angled off the rear of the nozzle or as normal shocks located inside it. As the backpressure increases even further from the ideal, the oblique shocks turn into normal shocks and travel upstream into the nozzle. Shock waves within the nozzle adversely interact with the boundary layer to cause complex flow disturbances and separation, leading to reduced thrust force along the walls and higher drag [4].

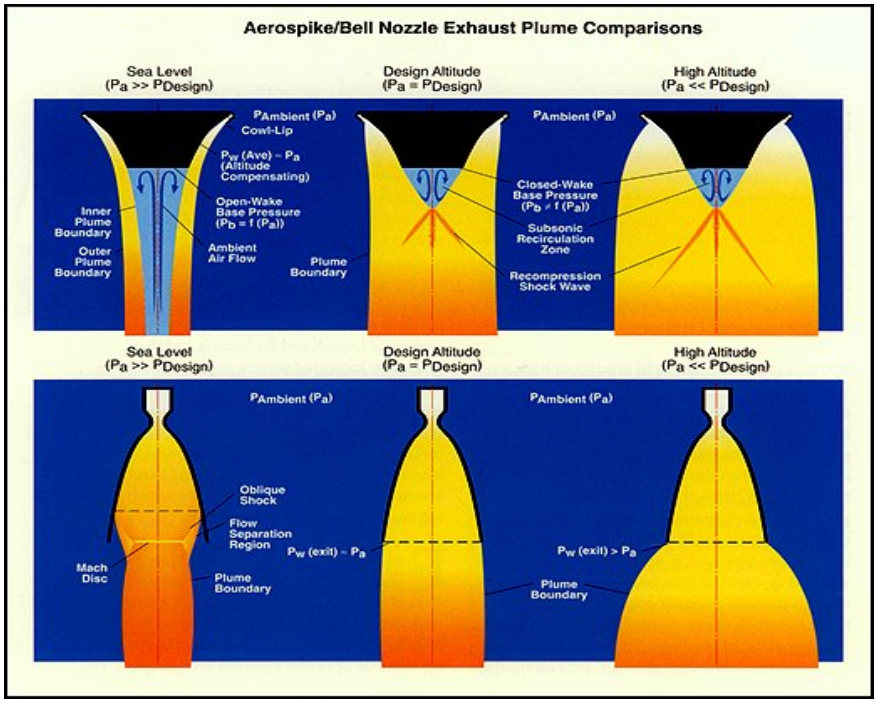

Figure 2: Comparison of C-D and Aerospike flow characteristics [4]

In nearly all practical applications, a launch vehicle will be subject to a wide range of ambient pressures during the course of its flight. In such cases, the C-D nozzle is designed for some intermediate pressure, with overexpansion occurring at sea level and underexpansion occurring at higher altitudes [4]. Designing the nozzle in this way minimizes the inefficiencies experienced at the extremities of the flight; however, the overall operation still remains inefficient. Investigations have been made into development of variable area-ratio nozzles, but the cost, complexity, and weight of such systems far outweigh the resulting increase in efficiency [2].

This less-then-optimum performance of current rocket technology is seen by some as being the limiting factor in being able to launch a meaningful payload into orbit with a rocket-powered SSTO craft [2]. The aerospike nozzle would be able to provide automatic altitude-compensation, all the while, requiring less nozzle length and weight for the same thrust [4]. For this reason, the AS nozzle is seen as a likely solution to making such a craft feasible [2].

The aerospike nozzle has a long, yet unspectacular presence in modern day rocket science. Originally, it was developed by the Germans during WWII in conjunction with the turbojet engine as a method for altitude-compensation. Later, during the 1950s, 60s, and 70s, the United States Air Force and the aerospace company Rocketdyne did extensive testing on plug and toroidal aerospike nozzles. During this time, an AS engine design was strongly considered for the Space Shuttle Main Engine. However, the cooling issues involved with the centrally located spike made the nozzle unrealizable for any practical application at the time. Today, renewed interest in the AS nozzle has been spawned out of the emerging SSTO concepts, most notably Lockheed Martin's cancelled, but still popular, X-33 and VentureStar programs. Currently, only a few, small-scale prototypes have been flown using an AS engine [2].

In general, AS nozzles are characterized as having thrust chambers located off the central axis surrounding a truncated, centrally located spike. The hot, high-pressure gases in the thrust chamber are accelerated to Mach 1 in the throat and are usually directed inward along the spike. The central spike has a profile similar to the bell nozzle, with the surface having a steeper slope near the throat that becomes asymptotic as it approaches the central axis [2]. Ideally, this spike should be of infinite length, but experiments have shown that when the spike is truncated and a small cold air flow is directed into the base of the spike, a low-pressure, circulating secondary flows forms. This secondary flow is energized by the shear interaction with the primary flow and acts to reduce drag and impart a thrust force on the base, resulting in only a 2% reduction in thrust from the ideal [4]. The secondary flow behaves as a virtual spike of infinite length, which is the root of the name "aerospike" [5].

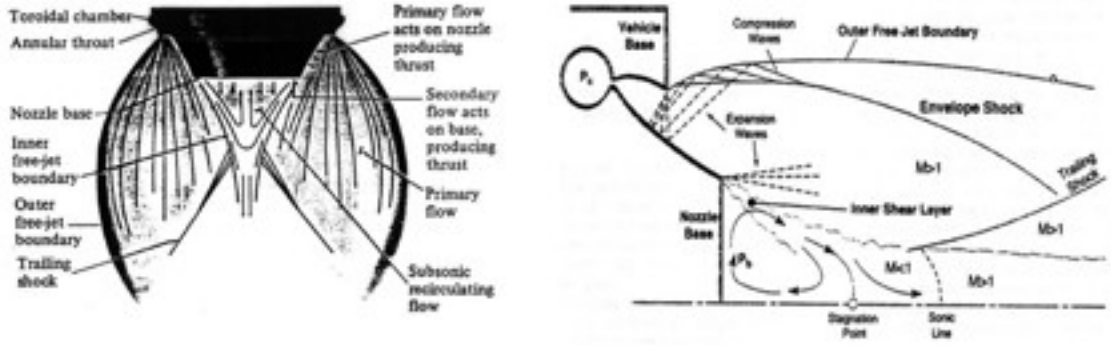

Figure 3: A 2-D visual of the aerodynamic flow field out of an aerospike nozzle [2]

The altitude-compensating capabilities of the AS nozzle comes from the fact that the gases leaving the throat are expanded externally, rather than internally like the C-D nozzle. The level of expansion is dictated by the ambient conditions rather than by the geometry of the nozzle. The freestream jet in contact with the outer plume boundary acts as a movable nozzle wall allowing the exhaust to expand against the spike as it reaches ambient pressure. During lower altitude operations, where the ambient pressure is higher than the pressure of the gas leaving the throat, the plume is curved inward along the spike and the plume area ratio formed by the virtual walls is kept small [5]. There are also additional effects that come into to play to increase the efficiency when operating at high backpressures. The expansion of the gases leaving the throat cause expansion waves which are reflected as compression waves off of the free plume boundary. At lower altitudes, the plume boundary is close enough to the surface of the spike to cause these compression waves to interact with the surface of the spike, which, due to the nozzle contour's gradual turning of the waves, serves to increase the overall pressure on the surface and contribute to the thrust. Also, these compression waves interact with the secondary flow to increase circulation, which increases the thrust imparted on the base [5].

As the altitude is increased, the outer plume boundary is allowed to move farther away from the spike's surface as needed, all the while, keeping the inner plume boundary firmly attached to the spike. The outer plume boundary takes on the shape of bell nozzle with an area-ratio appropriate to the altitude. As the ambient pressure is decreased, the compression waves move downstream until they no longer interact with the spike's surface.

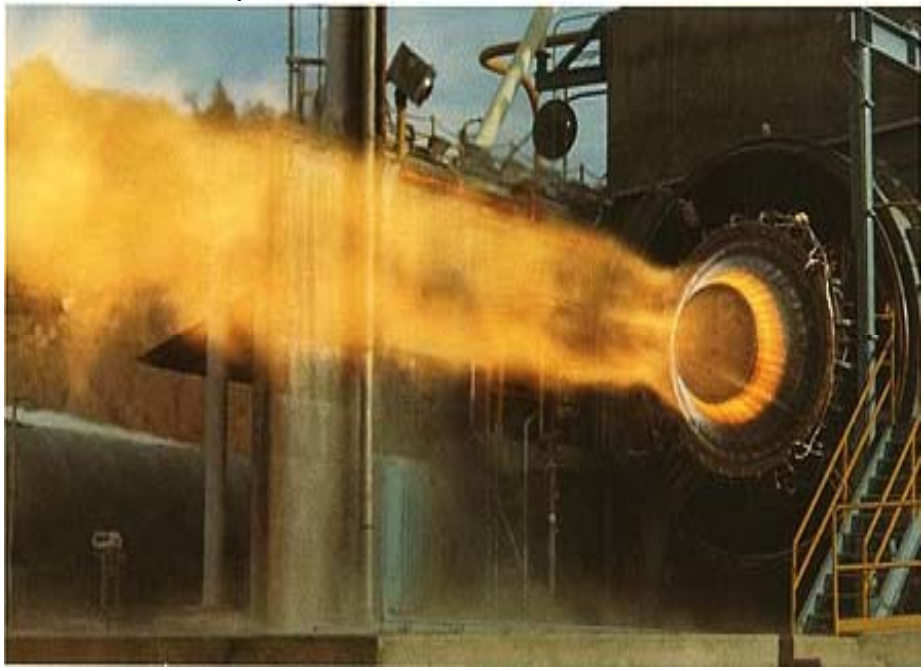

Figure 4: A view an outer plume of an annular aerospike nozzle [5]

At this point, the pressure distribution along the spike becomes constant regardless of the ambient pressure. At even lower backpressures, the compression waves act to close in the secondary flow region from the ambient conditions, causing the pressure distribution and thrust at the base to become constant. From this point on into true vacuum, the nozzle is said to have an enclosed wake and the thrust and efficiency vary little with changes in ambient pressure [2].

The AS nozzle takes on two forms: annular and linear. In the annular variant, exhaust is ejected from a toroidal thrust chamber onto a central spike. A more recent variant is the linear AS

nozzle. For this type, thrust chambers are arranged linearly along the thick end of tapered, wedge-shaped ramps. This design offers the ability to steer the craft with thrust vectoring, rather than with heavy, gimbaling mechanisms. Also, linear AS nozzles are modular and can be arranged in many different combinations [2].

Figure 5: A linear Aerospike in testing, "Lockheed, 2001"

By all accounts, the AS nozzle and its variants are believed to be able to approach the performance of C-D nozzles operating at optimum backpressures, while exceeding the C-D's performance at all other backpressures [4]. Some theoretical analyses have found the AS nozzle to exceed the C-D nozzle's performance even at its optimum backpressure [6]. In addition, the AS nozzle allows for reduced vehicle weight with shorter nozzle lengths and the absence of heavy gimbaling mechanisms. Also, AS engines require lower thrust chamber pressures than C-D engines to produce the same thrust, lowering the risk of catastrophic failure.

A major disadvantage of the nozzle is the cooling issues caused by the centrally located spike. A proposed solution to this has been to pump cryogenic fuel through the spike prior to being added to the combustor, similar to what is done in conventional rocket engines. Also, the addition of a small mass flow through the base does much to cool the spike [4]. Another disadvantage is the decrease in efficiency experienced by AS rocket powered vehicles at the flight speed range of Mach 1 to Mach 3. This is caused by the engines exhausting into the low-pressure region formed in the wake of the craft. The engine behaves as if it was operating at a higher altitude and some of the efficiency characteristic of low-altitude flight is lost. However, given that this range only encompasses a small portion of the flight, these losses are minimal [5].

For the most part, only limited amount of research has been done on AS nozzles and of that research, only a small portion includes actual flight tests. The intent of the experiment was to add to this limited research and, if possible, replicate the results achieved through other experiments and theoretical analyses. In this experiment, the thrust produced by a cold-gas, AS nozzle was tested against the thrust produced by a typical, bell-shaped, "de Laval" C-D nozzle as a function of altitude. In addition, a computational fluid dynamics model of the experiment was performed using FLUENT, in which a 2-D profile of the C-D nozzle was tested for conditions mimicking those experienced during the experiment. The results from the CFD simulation were used as a third point of comparison to validate the experimental results.

This experiment was performed as part of the 2007 High Altitude Student Platform (HASP) program. The HASP program was developed as a collaboration between the NASA Balloon Program Office (BPO), the Columbia Scientific Balloon Facility (CSBF), Louisiana State University (LSU), the Louisiana Board of Regents (BoR), and the Louisiana Space Consortium (LaSpace) with the goal of giving student groups access to near-space environments for extended durations at intermediate altitudes not achievable by low altitude balloons and low Earth orbit rockets. The platform is designed to carry up to twelve student payloads to a maximum altitude of about 36 kilometers. Using a zero-pressure polyethylene film balloon, the platform typically has flight durations ranging from 15 to 20 hours. This provides the capability for thorough testing and data-collection extended periods of time and for a wide range atmospheric conditions.

Team Structure

The HASP team consisted of seven individuals. Some of the team members contributed in a specific area of the project while others took more of a comprehensive role. The project student leader was Jeff Kornuta who along with Matt Hoenscheutz designed and fabricated the Main Control Unit of the entire experiment. The thrust stand and nozzle assembly were design by Theodore Bounds, John Dykes, and Edward Scheuermann. Ed was in charge of manufacturing these components, and CAD drawings of the thrust stand can be seen in the appendices. Henry Hardee and Ian Walsdorf were in charge of the design layout and system integration and calibration. Henry, Ian, John, and Jeff all played roles in troubleshooting and testing phases.

Experimental Apparatus

As previously stated, the objective of this experiment was to determine and compare the efficiencies of two different nozzles as the environmental conditions varied with altitude. More specifically, what is their behavior as the ambient (back) pressure changes? In order to safely and effectively test the two nozzles, an apparatus was designed with a number of fundamental requirements: a supply of power, a supply of propellant (air or other inert gas), a means by which to electronically control the experiment, and a means by which to extract the desired information and store this information as data. Additionally, the design needed to satisfy conditions specified by the HASP Student Payload Manual. One purpose of this manual is to provide more specific design constraints that will ensure maximum compatibility of the payload with HASP. Some of the more important constraints include spatial and weight limitations.

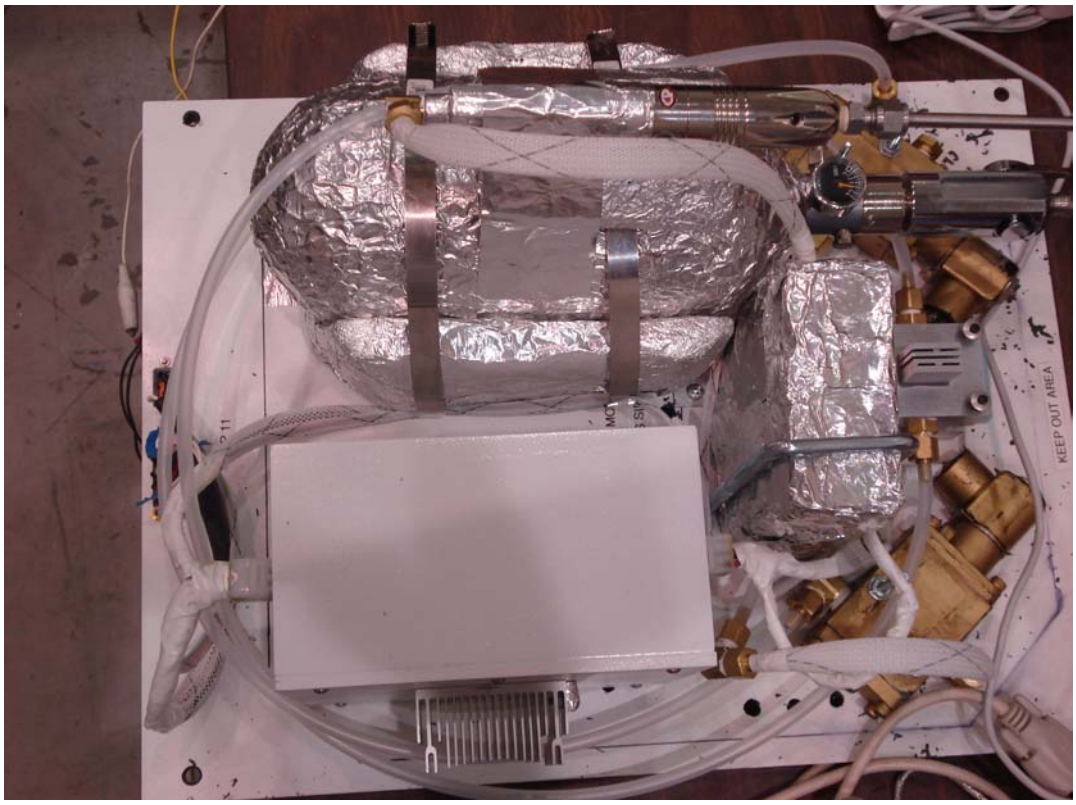

Figure 6: Top view of the entire experimental apparatus

The power supply was the most simple design task to be addressed. The HASP central power system provided 28 volts of DC current with a maximum current draw of 2.5 amps from an EDAC 516 twenty pin Connector as shown below in Figure 7. Before this energy can be utilized properly, the voltage must be stepped down to a voltage that is within the operating limits of each electronic component on the payload. The maximum operational voltage of any electronic component in the system was 5 volts, and the overall maximum voltage used was 12 volts by each of the two solenoid valves. Thus, a 12 volt switching voltage regulator and a 5 volt linear voltage regulator were utilized. For smaller components, passive elements such as resistors and capacitors were strategically placed for optimal operation.

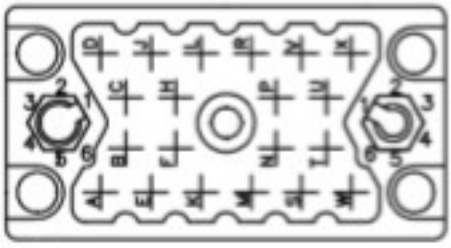

Figure 7: The EDAC 516–020 receptacle pin layout

Most of the electronic components used on the payload collectively make up the automated control system for this apparatus termed the Main Control Unit (MCU). A Parallax Basic Stamp BS2p24 microcontroller is the intellectual center of the system and effectively controls the experiment by making use of the variety of sensors and control elements. In addition, the MCU is able to collect data measured by several of the systems' sensors and locally record the data. For redundancy, the MCU also transmits collected data serially to be recorded by HASP. The MCU components are arranged optimally to occupy a custom-designed PCB board.

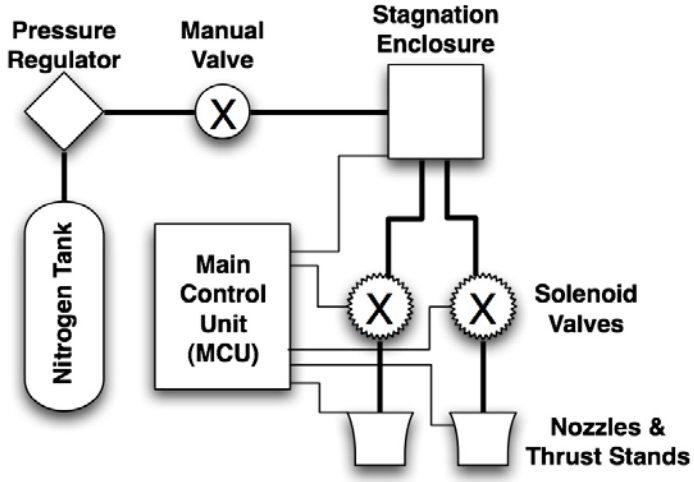

Figure 8: Payload schematic.

The team designed its own circuit board for a number of reasons. First, the design was modeled from a proven design that was developed by the LSU Physics Department. LSU Physics developed this board to be used with the LaACES ballooning program [9], and it has been utilized successfully a number of times. Additionally, a PCB board promotes good design methodologies since the development process demands a logical and methodical approach. Lastly, development of a PCB board allows duplicates of the MCU to be created quickly and easily.

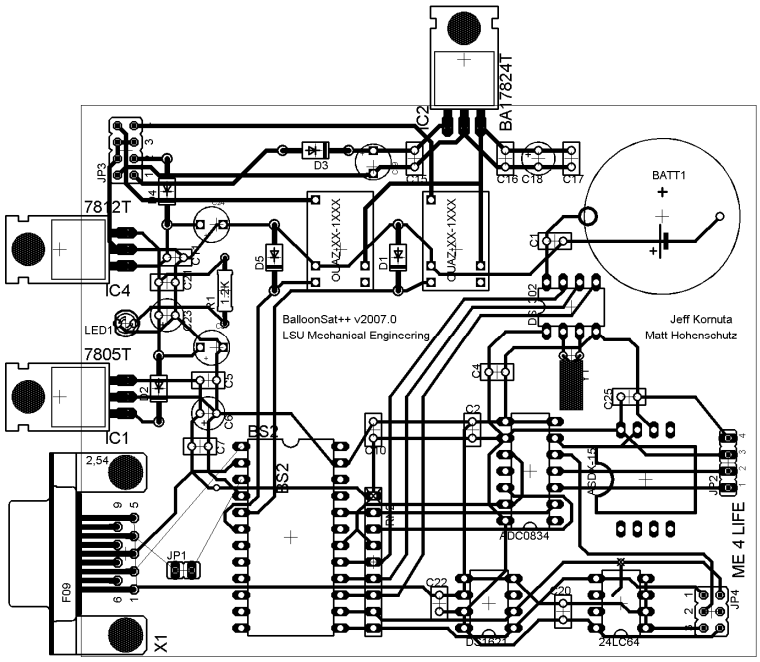

Figure 9: The prototype circuit board designed by team members Jeff Kornuta and Matt Hoenscheutz.

The circuit board utilizes several electronic components. Some of the more important components are a real-time clock, EEPROM memory, and a four channel 8-bit ADC. In order to ensure proper timekeeping, the RTC is provided with an independent 3 volt Lithium-ion battery in the event of a power outage. Also, the MCU's software algorithm is designed such that no data in the onboard memory is overwritten in the event of a sudden loss of power to the system. These safety precautions help minimize the chance of data loss and help increase the reliability of the system.

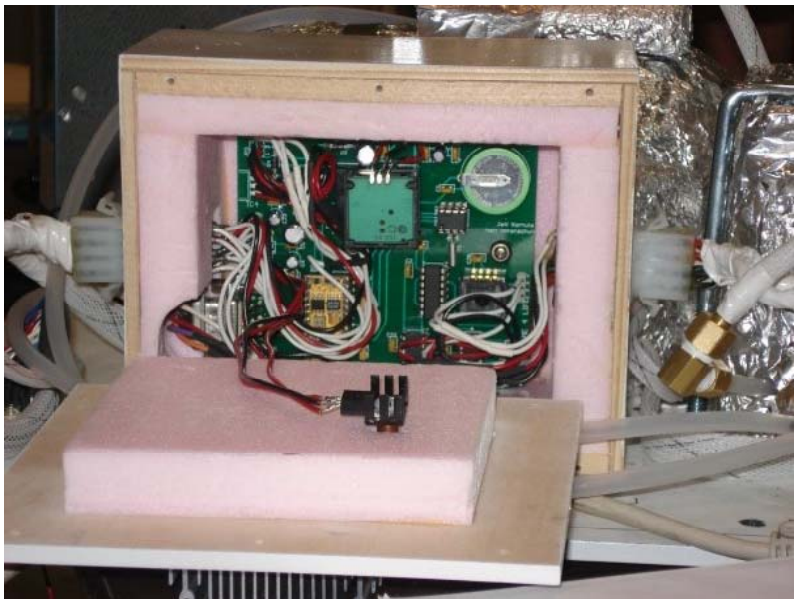

Figure 10: A view of the circuit board after being securely mounted in the insulated housing

The gas propellant is provided by a 4500 psia, 63 cubic inch carbon-fiber nitrogen paintball tank manufactured by Crossfire Inc. Directly attached to the tank is an 800 psia pressure regulator

and a manual on/off valve. Attached to this valve is another pressure regulator adjusted to 75 psia that leads to a splitter, which separates the flow into each of the two solenoids valves. From this point, each of the solenoid valves is directly attached to the thrust stand with flexible tubing.

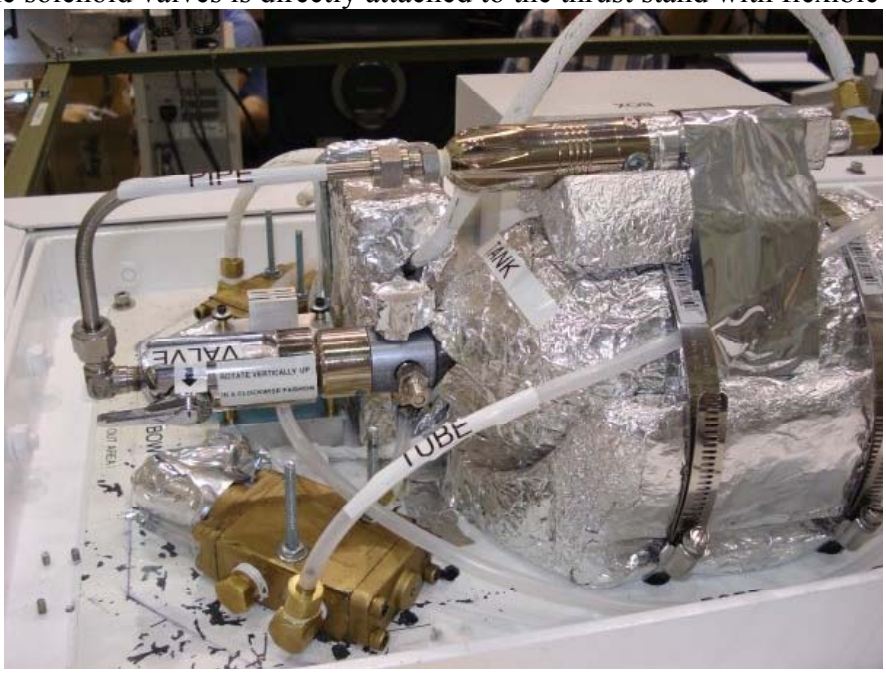

Figure 11: The design apparatus after being fully integrated into the HASP balloon chassis

During operation, an onboard 0-15 psia pressure sensor monitors the ambient conditions and informs the MCU when to execute the command for the thrust testing of each nozzle in order to ensure an evenly distributed data set with ambient pressure. In the course of a test, the ambient pressure and MCU enclosure temperature are recorded, and each of the solenoid valves are commanded to open and then close. During the brief period of time when the valve is open for each nozzle, the stagnation pressure, stagnation temperature, and thrust is recorded with a 0-100 psia pressure sensor, digital temperature sensor, and 5 lb compression-type load cell, respectively. The data is recorded locally and transmitted to HASP serially, and then the payload continues this cycle until an approximate vacuum is reached.

The thrust stand is a single, symmetrical unit that includes both the C-D and AS nozzle. Two flexible polypropylene tubes feed nitrogen gas into each side of the stand, and below the top portion of the stand rests the compression-type load cell.

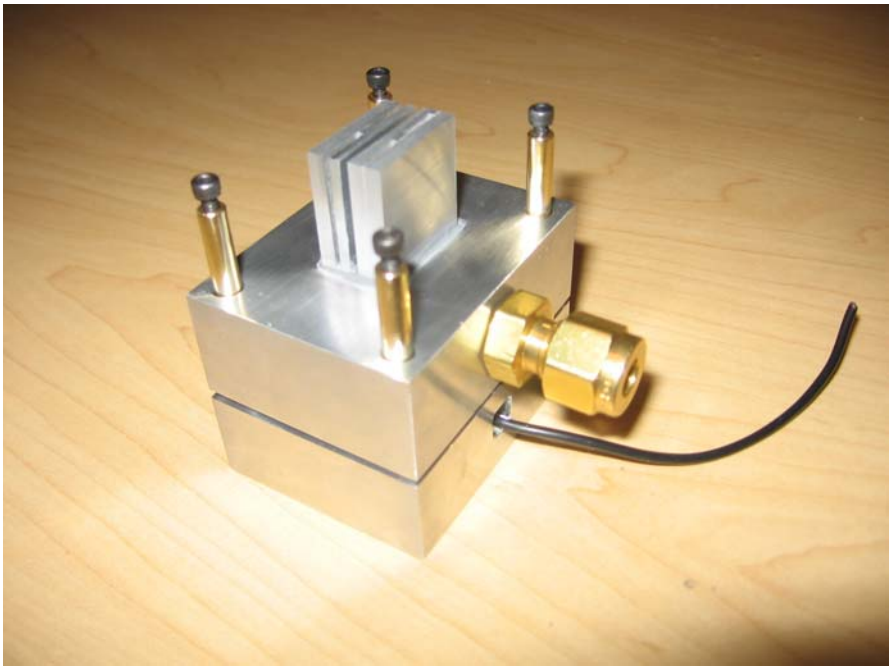

Figure 12: The thrust stand with both of the nozzles installed

By measuring the transient response of the nozzles and top portion of the stand with the load cell, a relatively good estimation of the thrust force can be found. Also, since both nozzles have equivalent throat areas and use the same thrust stand and load cell, the data collected from the two nozzles can certainly be compared.

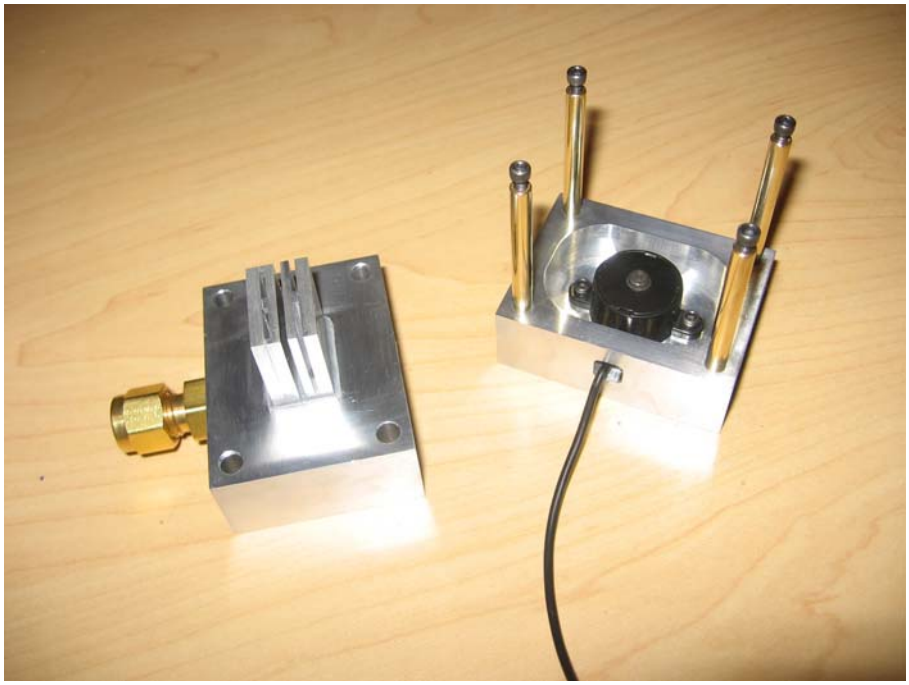

Figure 13: A view of the 5 lb load cell

Analytical Results

Experimental Results

The experimental results were divided into 50 subgroups (or trials) for analysis. These 50 subgroups are associated with a certain ambient pressure of the environment and include categories such as: the timestamp, temperature and pressure readings, as well as force/thrust readings. Since the HASP payload was launched at near sea level conditions (approximately 14.7 psi), and ambient pressure in space is near 0 psi, each trial of the experiment accounts for a change in the ambient pressure of approximately one fiftieth of standard pressure at sea level or .294 psi.

During the experiment, multiple readings were taken of each category in series so that a statistical analysis would increase both the accuracy and the precision of the data. Values such as temperature and pressure were taken in groups of five while the force readings were sampled 35 times. The figure below shows the difference in the thrust between the aerospike and bell nozzles for an arbitrary trial number.

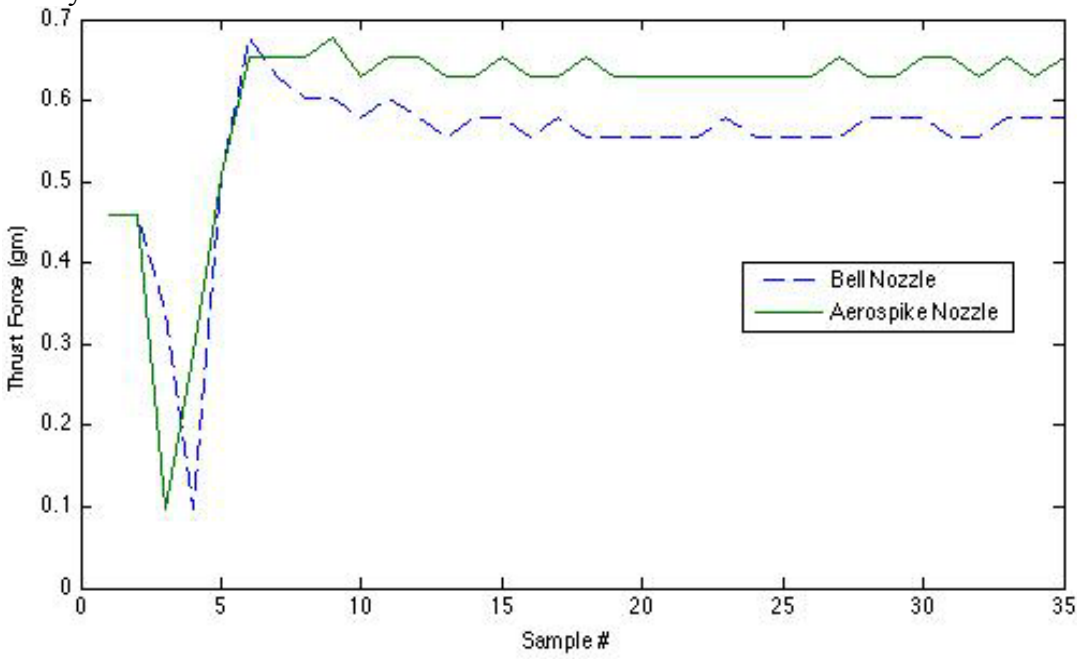

Figure 14: Thrust Force Readings for Trial #8, P_{amb} = 10.7 psi

From each trail, thrust forces were calculated for the two nozzles. This was achieved by recognizing that each of the force trends can be divided into three sections, as shown in figure 15. It is important to realize that these plots give the total forces that are experienced on the load cell. With that knowledge in mind, each section reveals different behaviors concerning these forces. In section 1, no gas has passed through a nozzle so this force reading only consists of the weight of the nozzles and thrust stand cap. It should be noted that the weight of this assembly changes throughout the experiment because the gravitational effect is much weaker on the object. Quantitatively, this can be explained by Newton's Law of Universal Gravitation, where the gravitational acceleration can be expressed as a function of altitude: $g(r) = -G\frac{m}{r}$. Since the radius of the earth is

approximately 6,370 km and the variation in altitude as the experiment progress is on the order of 38 km, the gravitation acceleration can be considered a constant average value. Section 2 represents the non-steady development of the flow as it begins to move through and out of the nozzle. This region was not considered in the thrust calculations due to its non-steady and irregular behavior between the 50 subgroups. The third section of the force readings is assumed to be the steady region. Therefore, the thrust was calculated by subtracting the statistical average (mean) of regions 3 from the mean of region 1.

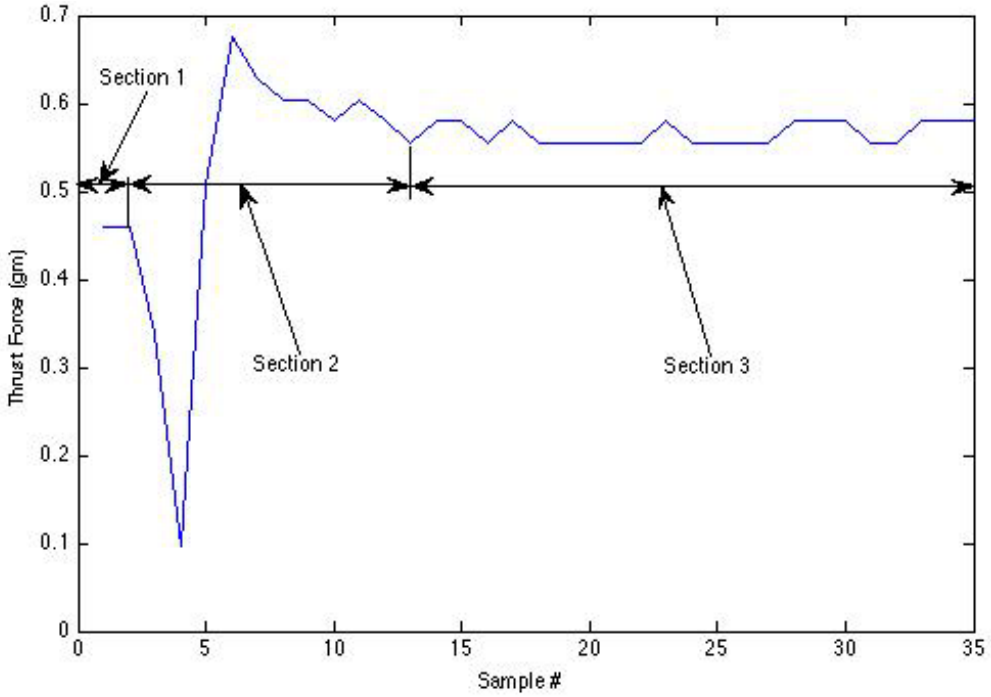

Figure 15: The three different regions of a force Reading

The thrust must be transformed into a dimensionless form via dimensional analysis so that variation can be limited to only one variable. For example, both the thrust measured by the load cell and the ambient pressure should vary as the experiment progresses. Note that because the tank was insulated, the change in temperature and thus density were sufficiently small were considered constant. The coefficient of thrust was calculated by the relation $C_T = \frac{T}{P_o A_e}$ [4], where P_o is the stagnation pressure and A_e is the exit area of the nozzles. In figure 16, the coefficients of thrust for the two nozzles are plotted as the ambient pressure varies throughout the earth's atmosphere.

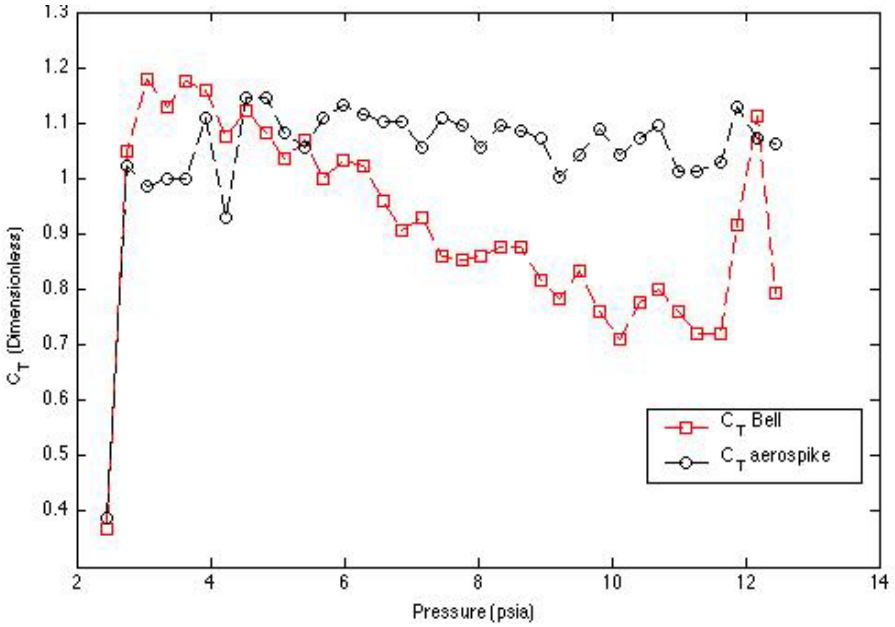

Figure 16: Thrust coefficients versus ambient pressure

Notice that values of thrust at pressures above 12.46 psi and below 2.24 psi were not recorded. This is due to corrupted data and errors in the experiment, which will be expounded upon later. Thus, not all 50 trials were recovered.

Temperature readings were recorded in order to validate the results shown above. By showing that the electrical components did in fact operate in the allowable range of temperatures, the error experienced in the electrical sensors was minimal. Below is a plot of the temperatures experienced inside the circuit housing as the ambient pressure of the outside environment changed.

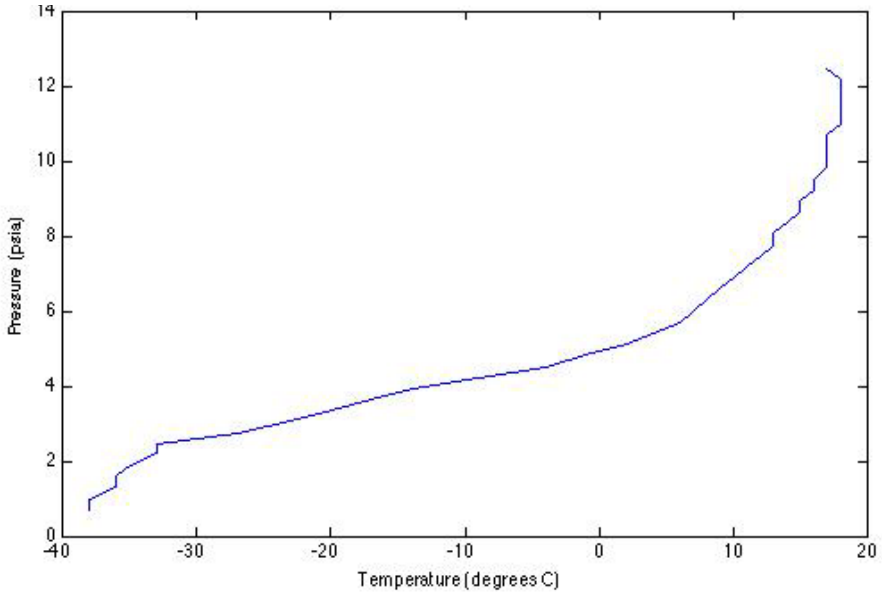

Figure 17: Temperature inside the circuit housing versus the ambient pressure

The minimum recorded temperature was close to -40^{o} Celsius. This is approximately the minimum allowable temperature of the components so this confirms that the operation of the electrical components is within the required range.

Discussion

Although the data at the beginning and end of the flight was corrupted, the extent of good data obtained was sufficient to describe the nozzles' performance for a wide range of ambient pressures. This range corresponds to roughly 65% of the total change in pressure experienced during the course of the entire flight.

As expected, the AS nozzle produced a relatively consistent thrust for every ambient pressure encountered. The coefficient of thrust averaged out to approximately 1.1006 with a standard deviation of only .0516. These results clearly show the aerospike nozzle's capability for altitude compensation.

The bell nozzle also performed as expected, producing significantly less thrust than the aerospike nozzle at lower altitudes. This inefficiency at low altitudes is consistent with overexpansion and inner flow separation due to the shock wave formation inside the nozzle. As the altitude increases and the balloon approaches the optimum backpressure, the thrust coefficient steadily increases. At an altitude around 8,000 m (26,000 ft), the bell nozzle overtook the aerospike in thrust and continued to increase further with altitude. Theoretically, the bell nozzle, which had an area-ratio of 4, would have achieved its optimum backpressure at roughly 17,000 m (56,000 ft) [8]. Unfortunately, the tank had lost pressure prior to reaching this altitude, so the maximum thrust for bell nozzle was never achieved. Based on extrapolation, the maximum thrust coefficient is approximately 1.35-1.4. Over the entire range of data, the bell nozzle had an average thrust coefficient of approximately .9647 with a standard deviation of .1486.

The experimental results for the bell nozzle agree, to some extent, with those gained through the CFD analysis. As seen in Figure 17, the fourth order polynomial curve fits of the experimental results for the bell nozzle and the analytical results follow very similar trends. Some differences between the curves are present. On the left hand side of the plot, the divergence between the two curves is due to the loss of pressure in the tank. On the right hand side, in the range of 8.5 to 13.5 psi, the divergence is due either to experimental error or to phenomena in the flow not adequately described by the simplified CFD model.

The experimental and analytical results for thrust coefficient as a function of altitude are shown in Figure 20. As with the previous plot, the analytical and experimental C-D nozzle values show similar tendencies (excluding the effects of experimental error). The CFD results in this plot specify the optimum altitude to be approximately 11,000 m (35,000 ft) based on examination of the generated curve. The point of optimum operation can be approximated to the point where the curve is subjected to a sharp change in the slope. In addition, this ideal operation can be seen in the velocity contours from the CFD shown in the appendix. The test for 11,000 m could not be performed due to issues with convergence, but this ideal operation is expressed well enough at the altitude of 12,000 m. At this altitude, shown in Figure 18, the exhaust plume takes on the ideal column shape and is absent of any shockwave formations. (Note: the tendency of the flow to pull to the left is due the strong, low-pressure region formed between the nozzles) This differs from the empirical calculation stated earlier, which specifies the optimum altitude (expressed as the vertical, dotted line in Figure 20) to be around 17,000 m (56,000 ft).

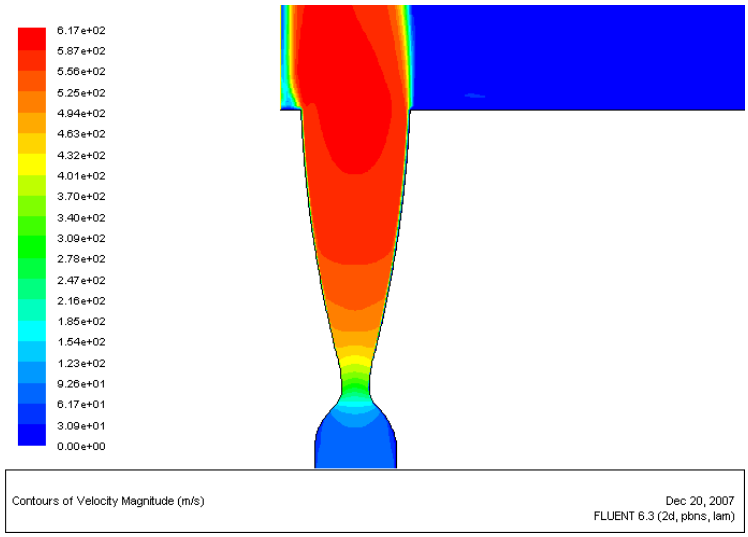

Figure 18: Velocity Contour from CFD analysis at 12000 m

These differences were expected to some degree. The CFD model was a simplified model meant to serve as a qualitative point of comparison for the experimental data. In this task, it was successful. The analytical model clearly shows that experimental data for the bell nozzle fits the expected behavior for a C-D nozzle with an area-ratio of 4 as a function of ambient pressure and, in doing so, validates the data. Given that the method for producing and measuring the thrust was identical for both nozzles, the model also validates the experimental data for the aerospike nozzle.

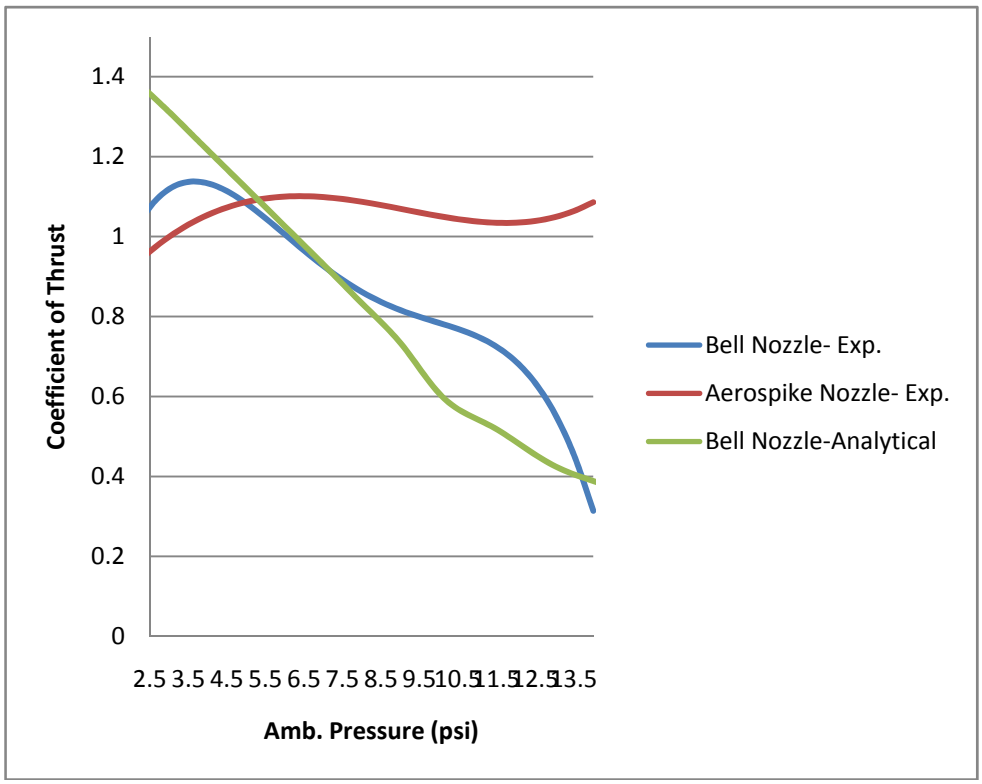

Figure 19: Trend lines for experimental and analytical coefficients of thrust as a function of ambient pressure.

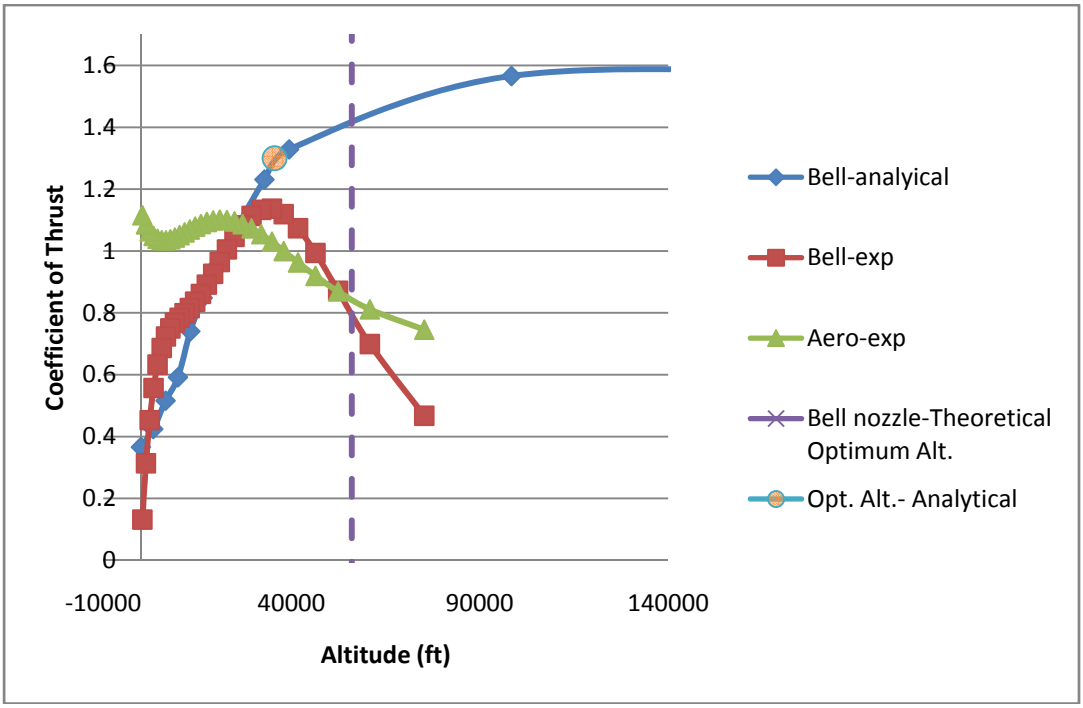

Figure 20: Coefficient of thrust versus altitude for experimental and analytical results.

Overall, the experimental results agreed with what was expected. The bell nozzle performed poorly at lower altitudes and gradually increased in efficiency with altitude. The aerospike nozzle produced effective, consistent thrust throughout the flight, but did not achieve the thrust of the bell nozzle operating at or near its optimum altitude. Theoretical data suggests that aerospike nozzles have the potential for matching the design-point performance of conventional nozzles [4]. This was not the case for these particular nozzles. However, the aerospike did achieve a 12.36% higher coefficient of thrust on average, which results in a significant advantage in overall efficiency.

Performance Assessment

The experiment had several mishaps that occurred during the flight of the experiment as previously mentioned. From the experimental data, it is evident that the apparatus did not function as expected near the beginning and the ending of the balloon flight. Upon investigation into these occurrences, it was concluded that the two accidents were independent of each other.

At the beginning of the experiment a number of issues were of concern. For example, wind patterns in the atmosphere could have caused vibrations that could have confused the sensors. Instrumentation error is a factor. There is also an issue concerning the thrust stand design. The brass pins upon which the thrust cap slides up and down on are made of brass. The rest of the thrust design was composed of 2024 Aluminum. This was done so that once the pins and cap were polished to a smooth finish, the cap would be able to very easily translate and not graze each other. Thus, the coefficient of static friction between the two would be at a minimal value for the entirety of the experiment. However, due to the required sensitivity, perhaps a linear bearing type design would have provided even more accurate results. Making use of this type of design would allow the reaction forces of the thrust to be almost purely transformed into the stress experience by the load cell and not lost to friction.

Figure 21: A small linear bearing, Wenling Huanyu Bearing Co., Ltd.

It is worth noting that this initial failure is a success for the design of the electronic control system. As previously mentioned, significant design considerations were invested into the fabrication of a prototype microcomputer circuit. This allowed for a small external power source that allows the programming algorithm to be able to recover from difficulties such as this. Theoretical results provide insight into where the data is valid and, thus, where the apparatus self corrects itself can be observed.

Near the end of the experiment, the results for both nozzles appear to plummet in value. The cause of this known and can be interpreted from figure 21.

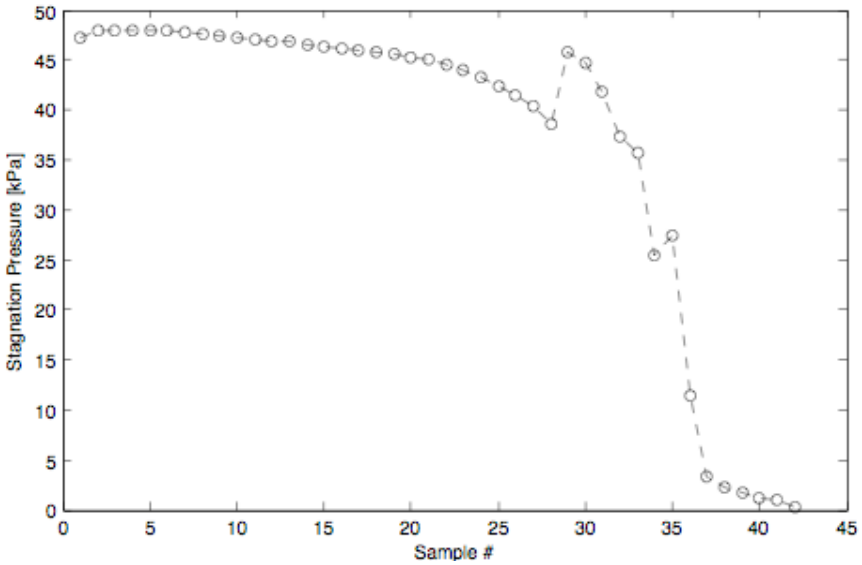

Figure 22: Stagnation Pressure throughout the experiment

After about 28 trials the pressure briefly spikes and then begins to fall. Perhaps additional testing would have allowed for fine-tuning of this aspect of the experimental design, but it is most probable that this drop off was due to a leak somewhere in the hydraulic system. Teflon tape was used to seal tubing at fittings, but this problem was a common occurrence during the testing phase.

In fact it was observed on a number of tests that a tube or fitting would spontaneously leak air after a number of trials were already performed successfully in a vacuum tank. The occurrences of these mishaps were substantially lessoned upon greater care being put into assembling the tubing network but unfortunately testing the apparatus in a various range of temperatures was never performed. Perhaps this additional testing could have allowed the design team to identify these problems beforehand.

Conclusions

An aerospike nozzle was tested against a conventional bell-shaped nozzle for thrust as a function of altitude. Interferences in the very beginning of the flight, caused by strong winds or the acceleration of the balloon, resulted in inaccuracies in thrust readings at low altitudes. In addition, premature loss of pressure in the supply tank halted data collection for the last half of the flight. Nonetheless, the satisfactory data that was collected spanned a majority of the total change in pressure experienced during the course of the flight and, as such, was sufficient to draw strong conclusions about the performance of the nozzles. As a result, the experiment was a reasonable success.

As expected, the aerospike nozzle demonstrated the ability to compensate for ambient pressure by producing consistent thrust at all altitudes. The bell nozzle also exhibited typical behavior with poor performance at low altitudes and a gradual increase in thrust to eventually overtake the aerospike nozzle as the optimum altitude was approached. Overall, the aerospike nozzle possessed a coefficient of thrust that was, on average, 12.36% higher than that of the bell nozzle over the course of the flight. In light of SSTO craft or any other craft that experiences changes in altitude, this would result in a significant gain in thrust efficiency, leading to higher payload capacities or range.

In addition to providing interesting and useful data on these highly experimental nozzles, this project imparted a wealth of knowledge and experience to each member of the design team. The environment surrounding high-altitude balloons is unpredictable and designing experimental apparatuses to perform in this environment is challenging, to say the least. In completing this project, the team members were challenged with advanced problems in rocket nozzle design, electronics, heat transfer, and CFD. In addition, the team also learned valuable lessons in project management and teamwork.

References

[1] Varvill, Richard and Bond, Alan, "A Comparison of Propulsion Concepts for SSTO Reusable Launchers", Vol. 56, pp. 108-117. *Journal of the British Interplanetary Society*, http://www.reactionengines.co.uk/downloads/JBIS_v56_108-117.pdf.

[2] Scott, Jeffrey A., "Aerospike Engine" http://www.aerospaceweb.org/design/aerospike/main/shtml.

[3] Fox, Robert W., McDonald, Alan T., and Pritchard, Philip J., Introduction to Fluid Mechanics. John Wiley and Sons, Inc., 2006.

[4] Hill, Philip and Peterson, Carl, Mechanics and Thermodynamics of Propulsion Addison-Wesley Publishing Company, 1992.

[5] O'Leary, R.A. and Beck, J.A., "Nozzle Design" *Threshold,* Spring 1992, http://www.engineeringatboeing.com/articles/nozzledesign.htm.

[6] Huzel, Dieter K. and Huang, David H., Design of Liquid Propellant Rocket Engines. Washington D.C.: NASA Science and Technical Information Office, 1967.

[7] Ruf, J.H. and McConnaughey, P.K. "The Plume Physics Behind Aerospike Nozzle Compensation and Slipstream Effect" AIAA Paper 97-3218, 1997.

[8] Anderson Jr., John D., Fundamentals of Aerodynamics., 4th ed., McGraw-Hill Companies, Inc., 2007.

[9] Louisiana Space Consortium, http://laspace.lsu.edu/aces/

Appendices

Matlab Data Analysis Program

```
%HASP '07 Data Analysis (Matrix Assignments, Conversions, & plots)
%Louisiana State University
%For: Dr. Shengmin Guo & Dr. T. Gregory Guzik
%By: John Dykes
clc
clf

%Start:skip initial activation sequence
x=185;

for i = 1:42 %(took 50 readings)
    %initial timestamp
    for j = 1:6
        z = raw_data(x,1);
        time_stamp(i,j) = z;
       %time_stamp(i,j)=Hex2Dec(z); %accending order (s-min-hr-d-mo-yr)
        x=x+1;
    end
    %temperature inside box
    for j = 1:5
        z = raw_data(x,1);
        if z >= 128
            z = -1*(256-z);
        end
        box_temp(i,j) = z;                      %Celsius
        x = x + 1;
    end
    %ambient pressure
    for j = 1:5
        z = raw_data(x,1);
        amb_press(i,j) = (15/204)*z - 15/8;          %psia
        x = x+1;
    end
    %stagnation temperature
    for j = 1:5
        z = raw_data(x,1);
        if z >= 128
            z = -1*(256-z);
        end
        stag_temp(i,j) = z;                     %Celsius
        x = x+1;
    end
```

```
    %force for zero nozzle
    for j = 1:35
        z = raw_data(x,1);
        force_zero(i,j) = .02416*z-.5556;            %lbf
        %force_zero(i,j) = 10.959*z - 252.016;       %grams
        x = x+1;
    end
    %stagnation pressure for zero nozzle
    for j = 1:10;
        z = raw_data(x,1);
        stag_presszero(i,j) = .4891*z - 12.5;        %psia
        x = x+1;
    end
    %force for 1 nozzle
    for j = 1:35
        z = raw_data(x,1);
        force_one(i,j) = .02416*z-.5556;             %lbf
        %force_one(i,j) = 10.959*z - 252.016;        %grams
        x = x+1;
    end
    %stagnation pressure for one nozzle
    for j = 1:10
        z = raw_data(x,1);
        stag_pressone(i,j) = .4891*z - 12.5;         %psia
        x = x+1;
    end
end
%Thrust force Calculations
A_cd = 0;
A_as = 0;

for i = 1:42
    for j = 1:2
        A_cd = A_cd + force_one(i,j);
        A_as = A_as + force_zero(i,j);
    end;
    lab_thrust(i,1) = A_cd/2;
    lab_thrust(i,2) = A_as/2;
    A_cd = 0;
    A_as = 0;
    for j = 30:35
        A_cd = A_cd + force_one(i,j);
        A_as = A_as + force_zero(i,j);
    end;
    lab_thrust(i,3) = A_cd/5;
    lab_thrust(i,4) = A_as/5;
```

```
    A_cd = 0;
    A_as = 0;

    lab_thrust(i,5) = lab_thrust(i,3)-lab_thrust(i,1);
    lab_thrust(i,6) = lab_thrust(i,4)-lab_thrust(i,2);
end;

%Pressure Calculations
A_cd = 0;
A_as = 0;
for i = 1:42
    for j = 1:10
        A_cd = A_cd + stag_pressone(i,j);
        A_as = A_as + stag_presszero(i,j);
    end;
    lab_press(i,1) = A_cd/10;
    lab_press(i,2) = A_as/10;
    A = 0;
    for j = 1:5
        A = A + amb_press(i,j);
    end;
    lab_press(i,3) = A/5;
    A_cd = 0;
    A_as = 0;
end;

%Dimensionless thrust force calculations
A_cd = 0;
A_as = 0;
Area_throat=4/(10*2.54)^2;  %in^2
for i = 1:42
    cf_one(i,1) = lab_thrust(i,5)/(Area_throat*stag_pressone(i,1));
    cf_zero(i,1) = lab_thrust(i,6)/(Area_throat*stag_presszero(i,2));
end
%%Plot Cf vs. P_amb
% clf
% x  = 34:-1:4;
%subplot(2,1,1)
% plot(lab_press(x,3),cf_one(x,1),'--rs',lab_press(x,3),cf_zero(x,1),'--ok')
%title('C_{T} vs. Ambient Pressure')
% legend('C_T Bell','C_T aerospike')
% Xlabel('Pressure (psia)')
% ylabel('C_{T} (Dimensionless)')
%axis([0,15,.4,1.2])
% %%Plot T_amb vs. P_amb
% x = 1:1:41;
```

```
% subplot(2,1,2)
% plot(stag_temp(x,1),lab_press(x,3))
% title('Temperature inside the box vs. Ambient Pressure')
% Xlabel('Temperature (degrees C)')
% Ylabel('Pressure (psia)')
% %%plot of a force output
% clf
% plot(1:35,force_one(18,1:35))%,'--',1:35,force_zero(8,1:35))
% %legend('Bell Nozzle','Aerospike Nozzle')
% %title('A')
% Xlabel('Sample #')
% Ylabel('Thrust Force (gm)')
%%plot of stagnation pressures
x = 1:1:42;
plot(x,lab_press(x,1),'--ok')
xlabel('Sample #')
ylabel('Stagnation Pressure [kPa]')
```

C AD Drawings

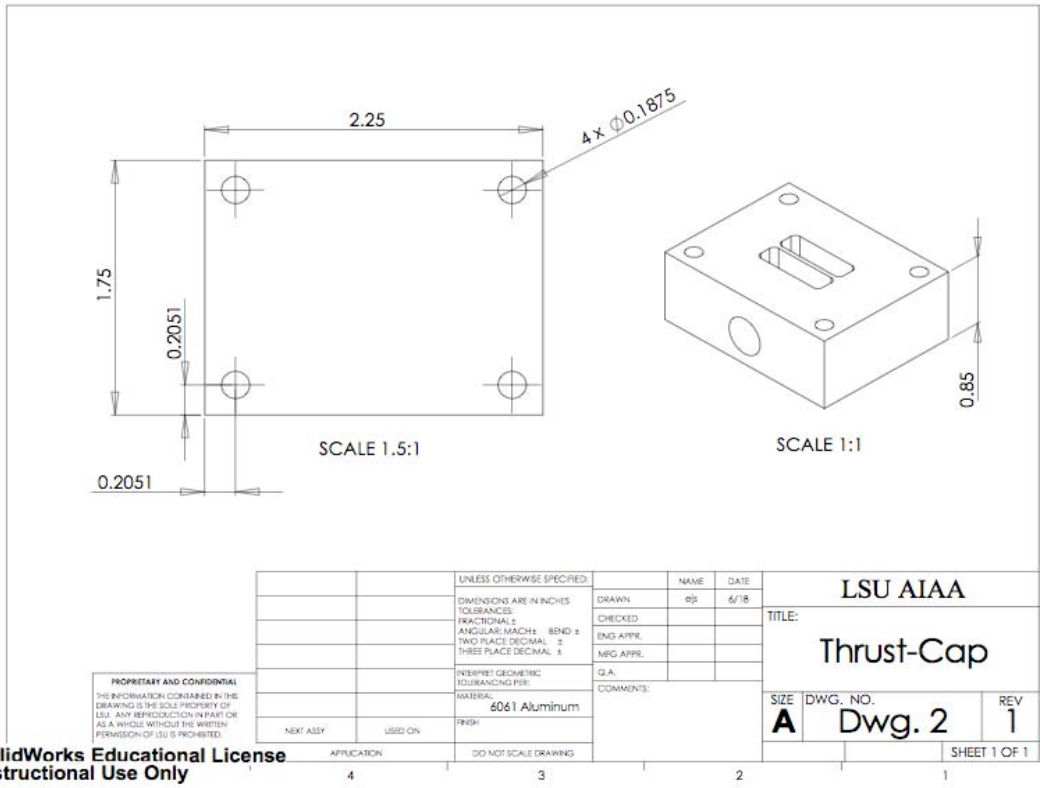

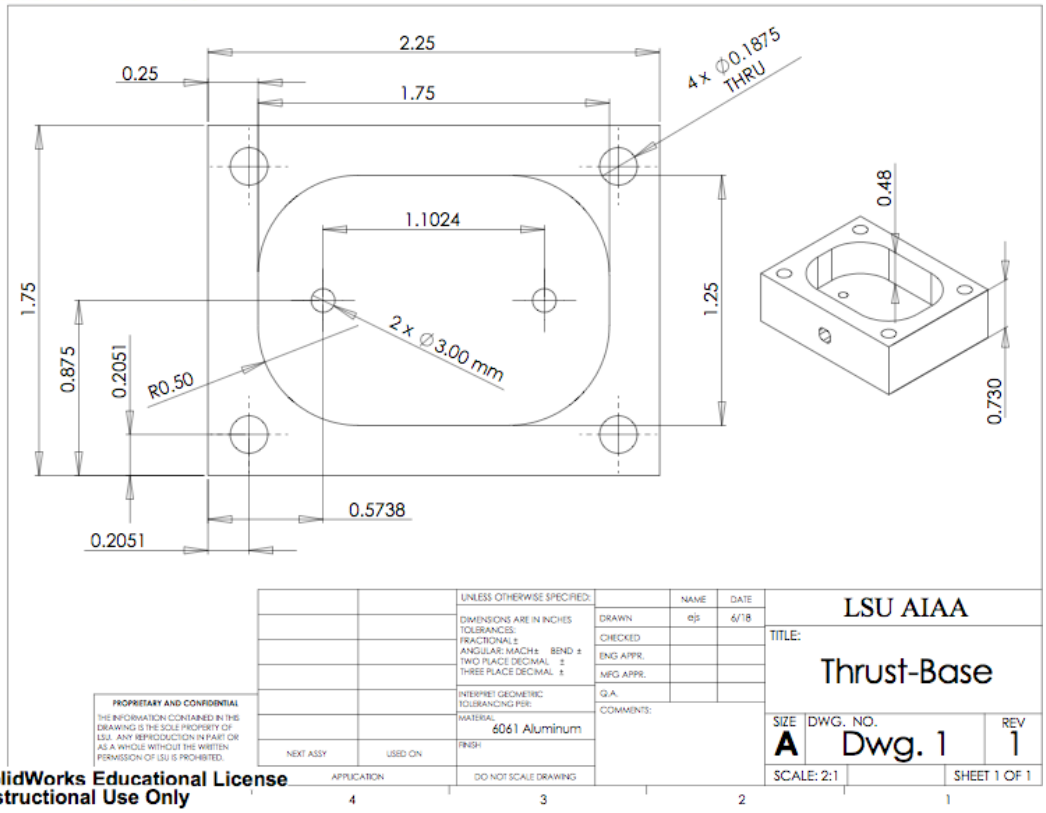

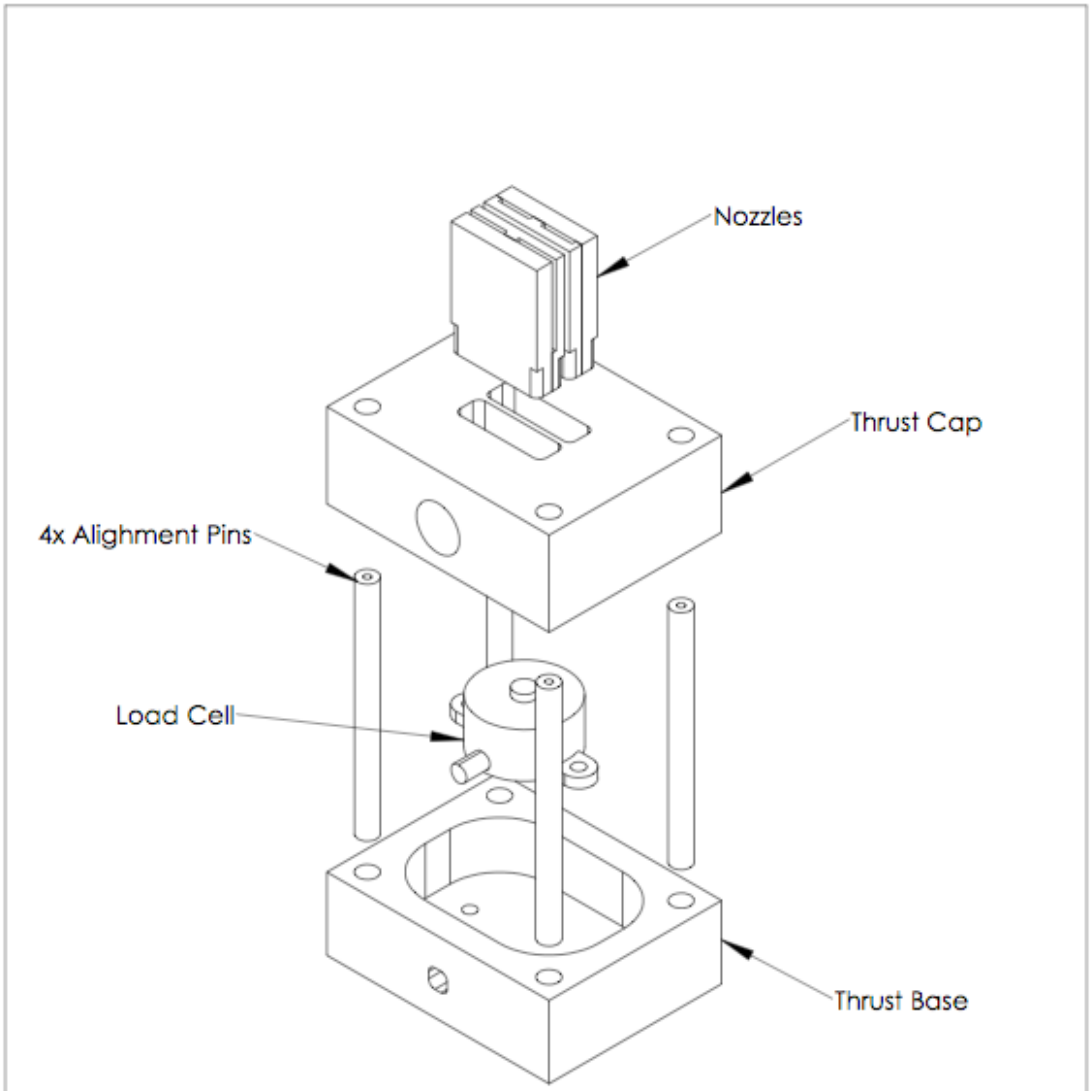

		DIMENSIONS ARE IN INCHES TOLERANCES: FRACTIONAL ± ANGULAR: MACH ± BEND ± TWO PLACE DECIMAL ± THREE PLACE DECIMAL ±		NAME	DATE
			DRAWN	ejs	6/18
			CHECKED		
			ENG APPR.		
			MFG APPR.		
		MATERIAL	Q.A.		
NEXT ASSY	USED ON	FINISH	COMMENTS:		
		DO NOT SCALE DRAWING			

LSU AIAA

Thrust Assembly

SIZE	DWG. NO.	REV.
A	Assembly-Exp	1

SCALE: 1.5:1 SHEET 1 OF 1

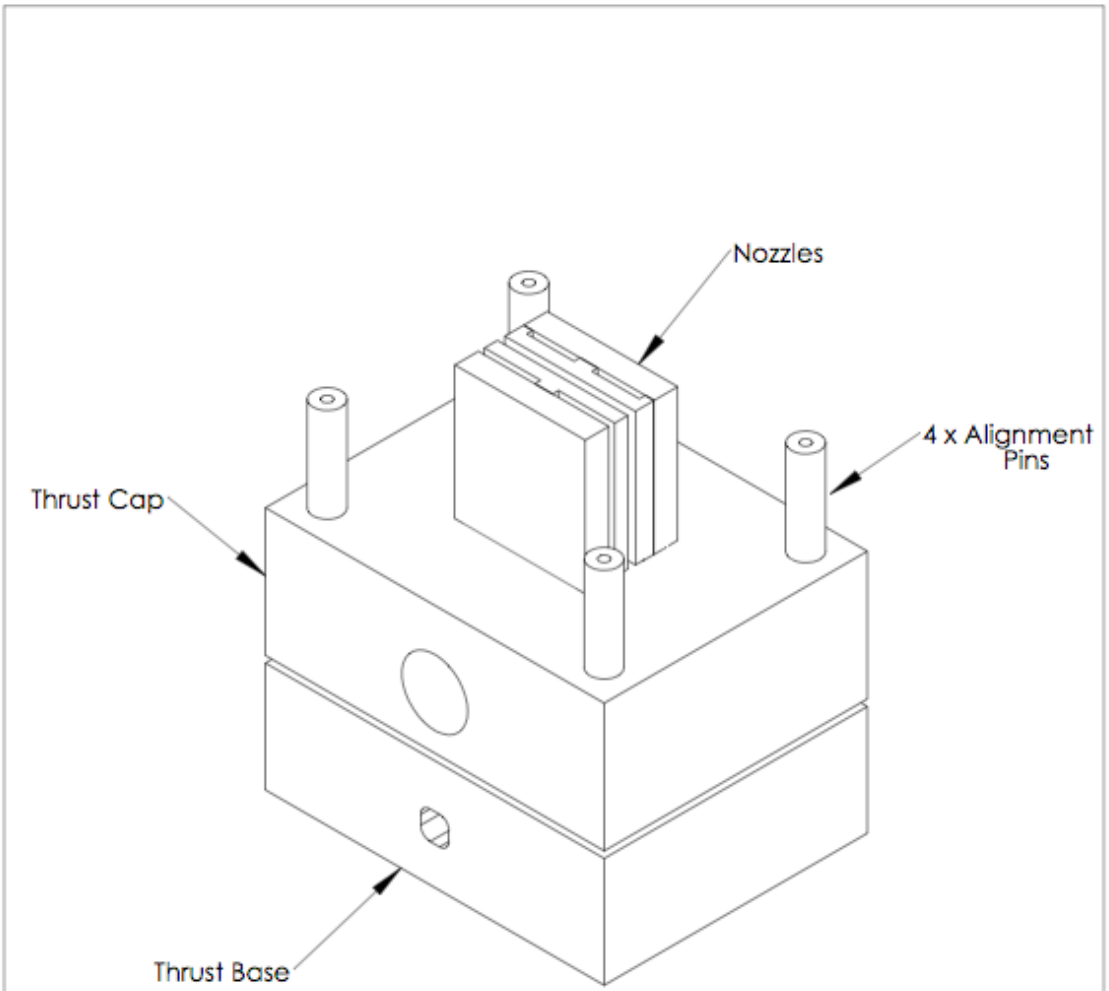

		DIMENSIONS ARE IN INCHES TOLERANCES: FRACTIONAL ± ANGULAR: MACH ± BEND ± TWO PLACE DECIMAL ± THREE PLACE DECIMAL ±		NAME	DATE	LSU AIAA	
			DRAWN	eg	6/18		
			CHECKED				
			ENG APPR.				
			MFG APPR.				
			Q.A.				
			COMMENTS:				
		MATERIAL				Thrust Assembly	
		FINISH					
		DO NOT SCALE DRAWING				SIZE A / DWG. NO. Assembly / REV. 1	
						SCALE: 1.5:1	SHEET 1 OF 1

Design Schematics

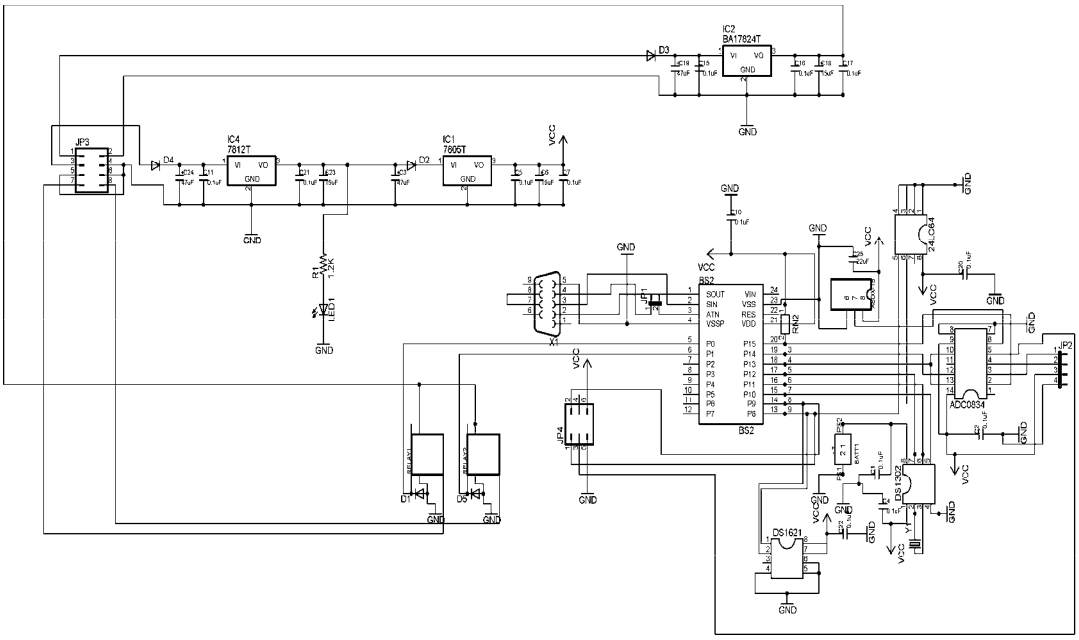

Figure 23: This is a schematic diagram of the BalloonSat.

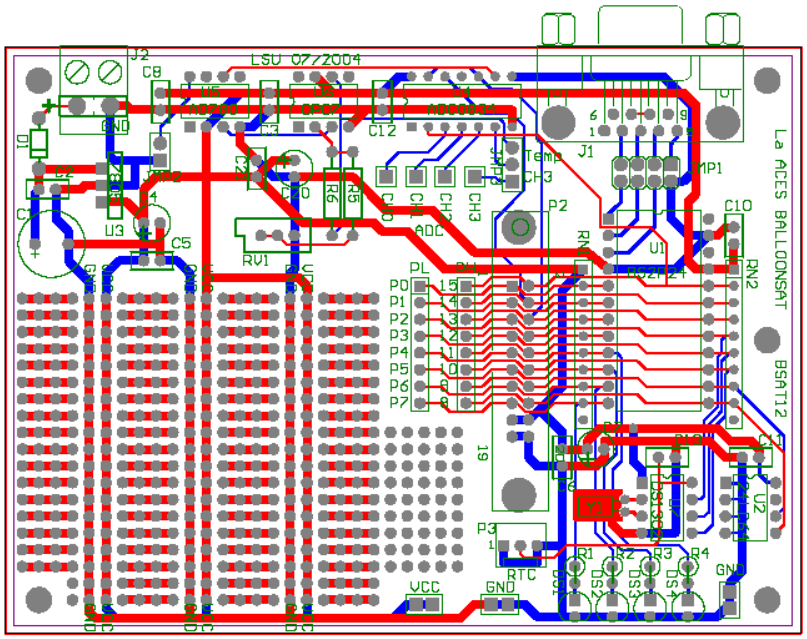

Figure 24: The LaACES Balloonsat microcontroller circuit board layout.

FLUENT® Analysis

Velocity

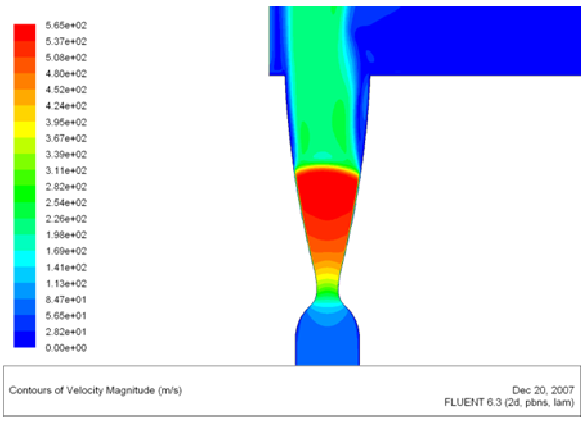

0 m

Pressure

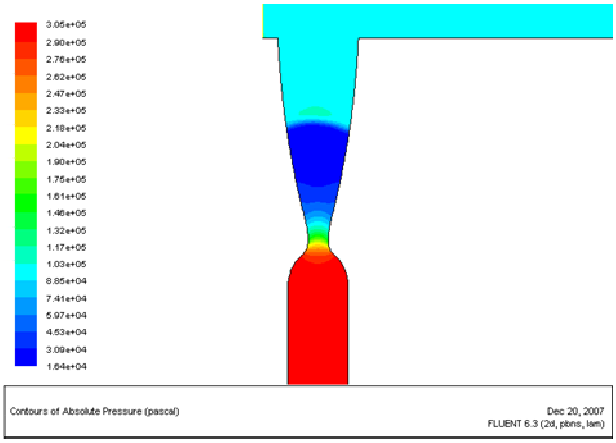

0m

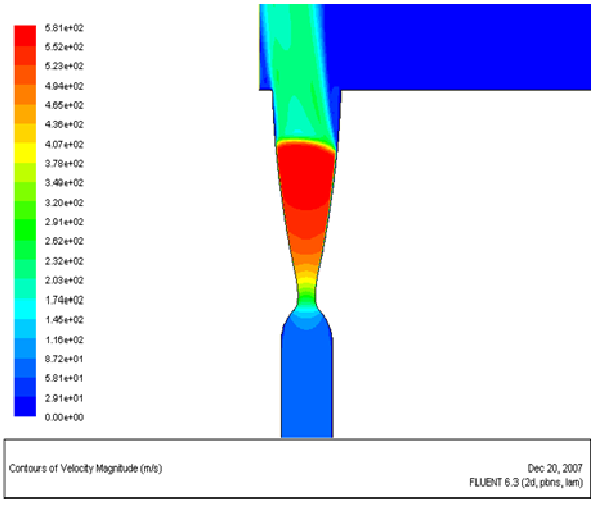

1000m

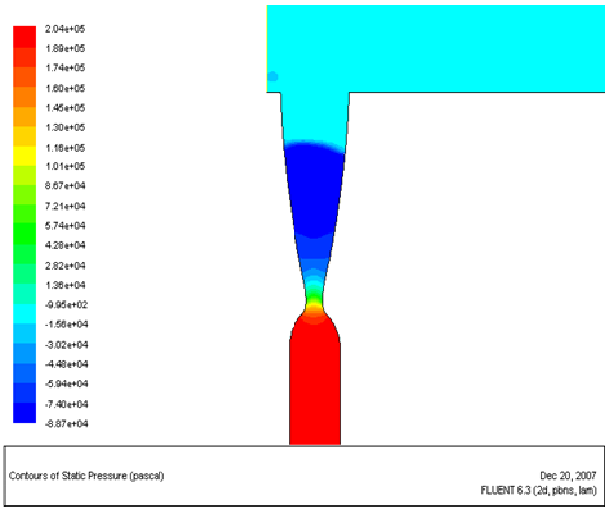

1000m

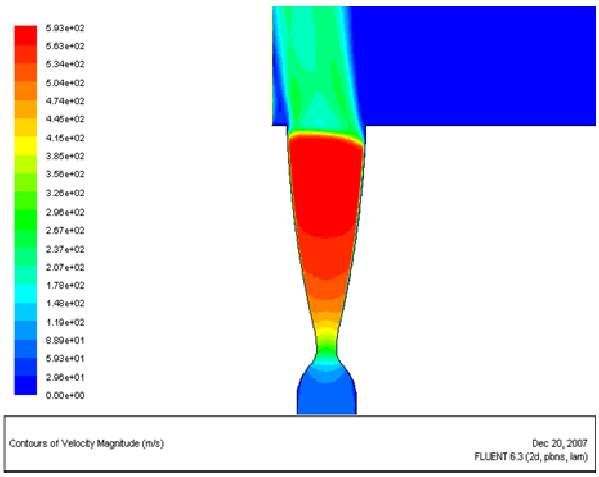

2000m

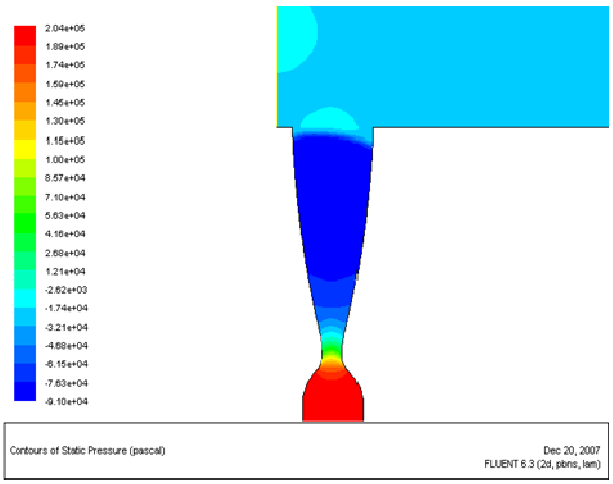

2000m

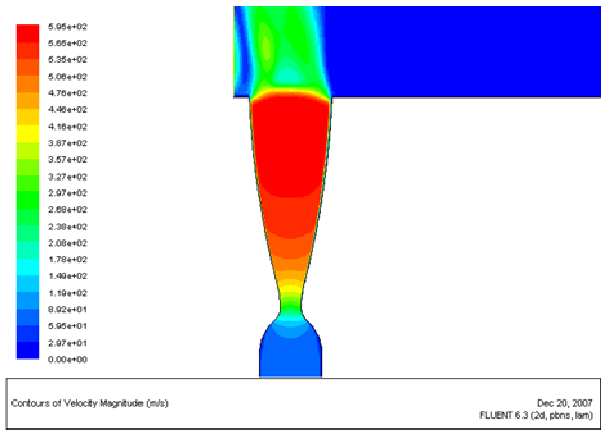

3000m

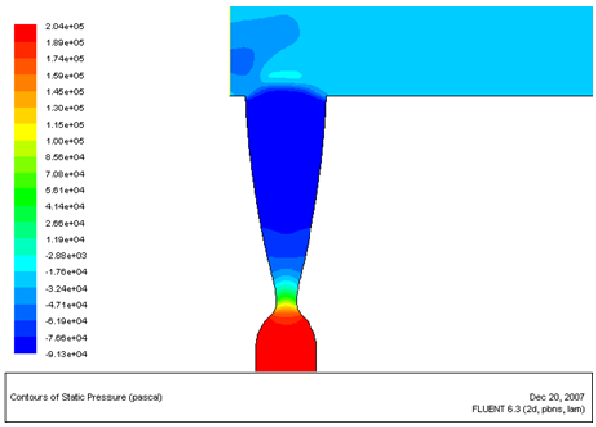

3000m

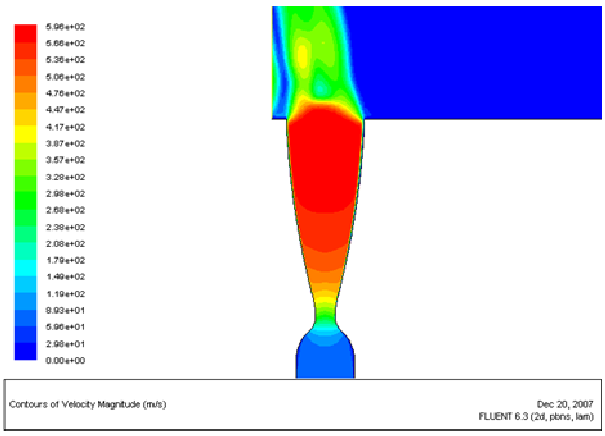

4000m

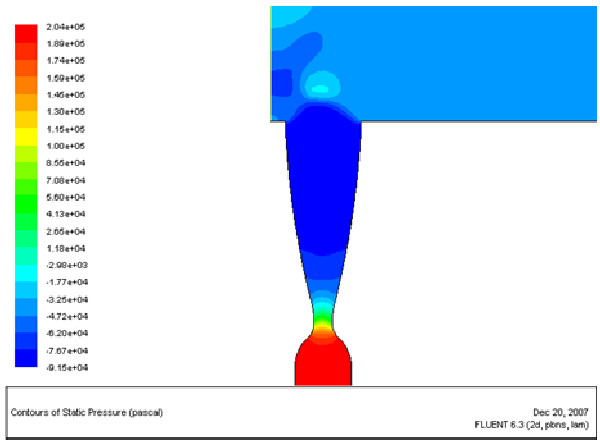

4000m

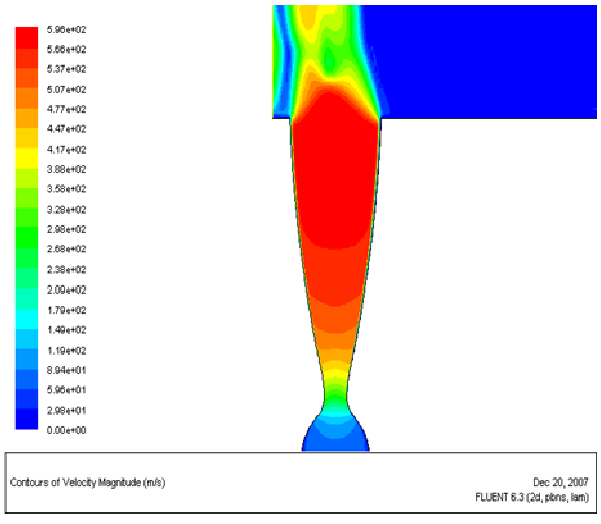

5000m

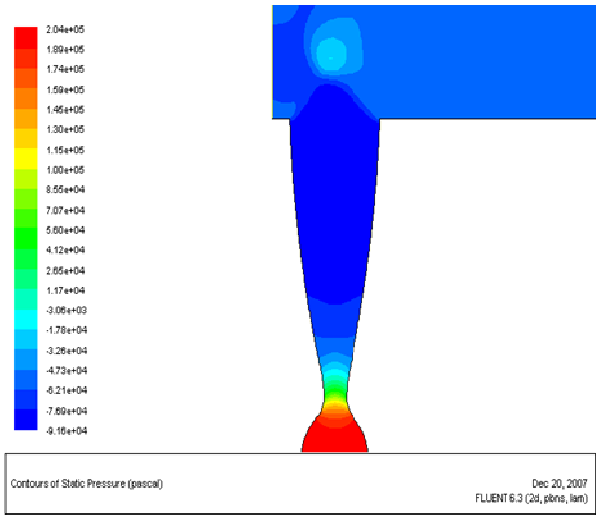

5000m

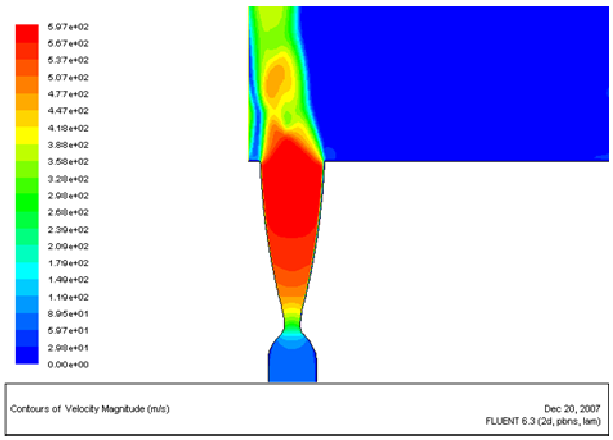

6000m

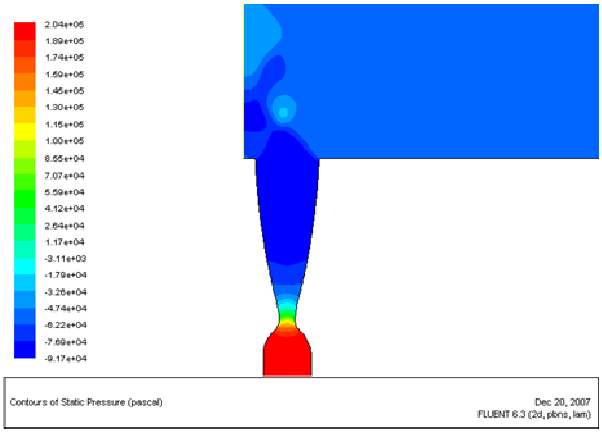

6000m

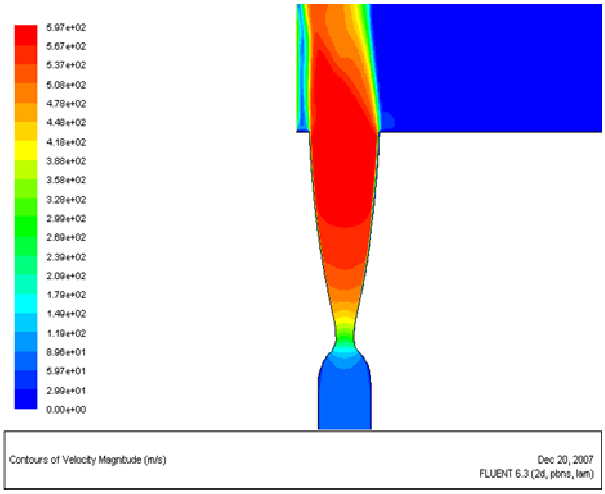

10,000m

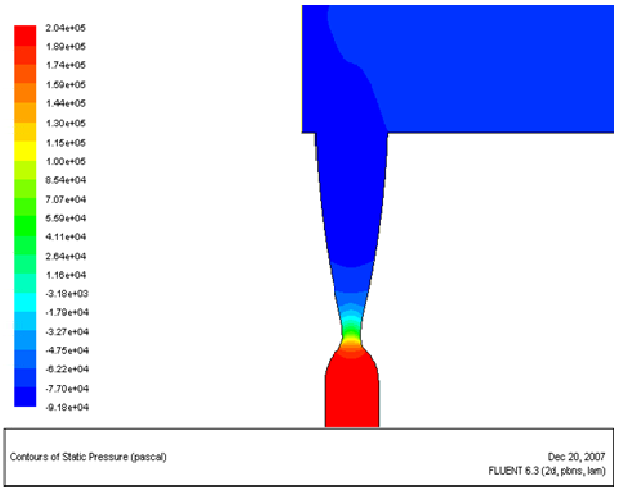

10,000m

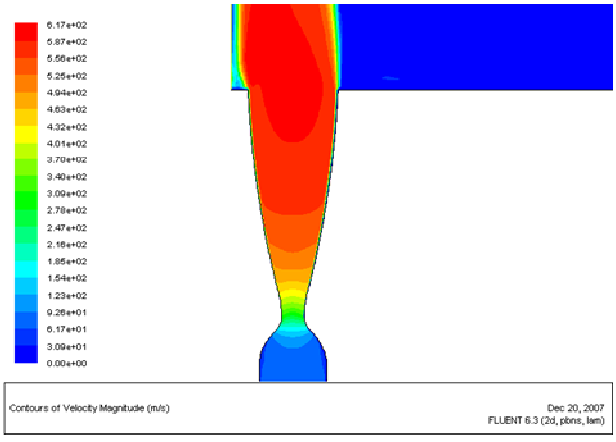

12,000m

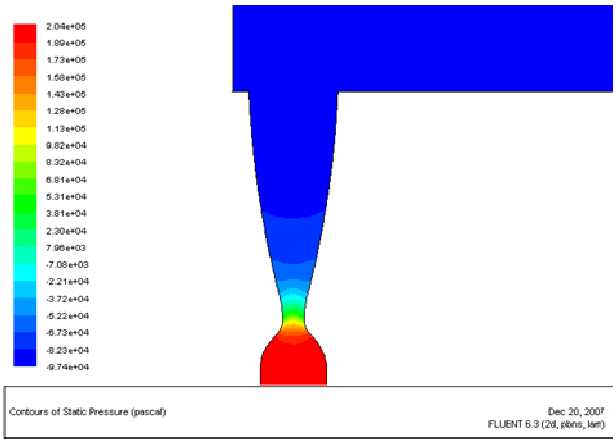

12,000m

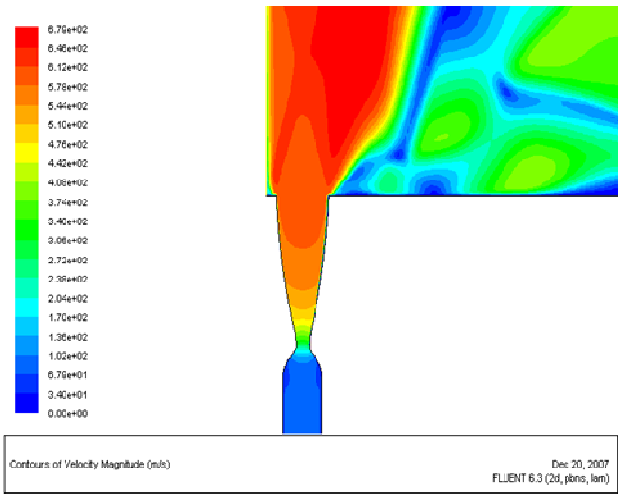

30,000m

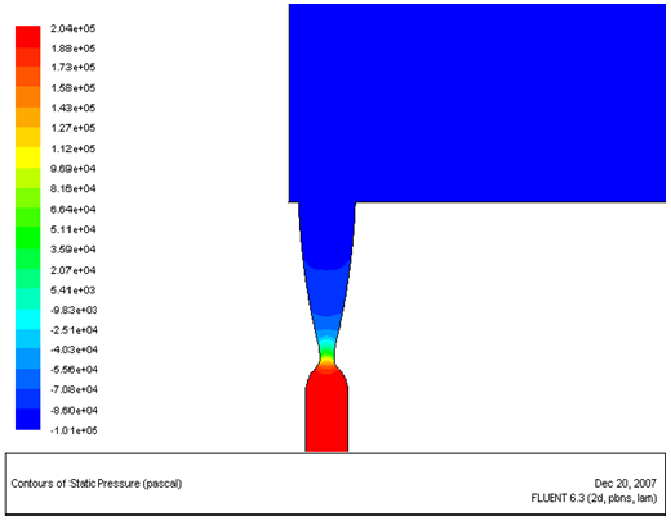

30,000m

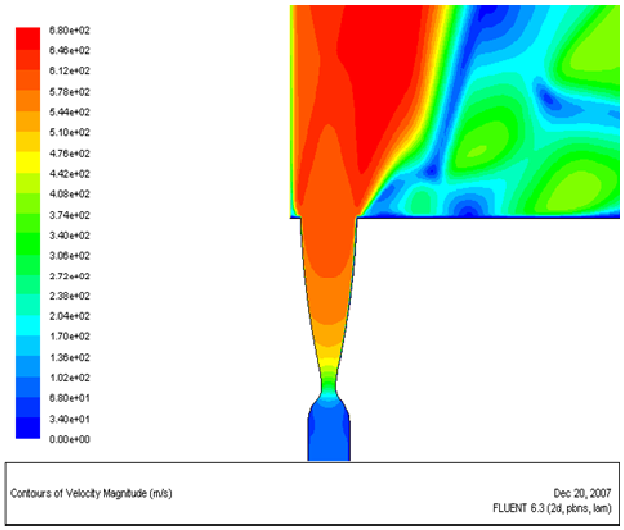

60,000m

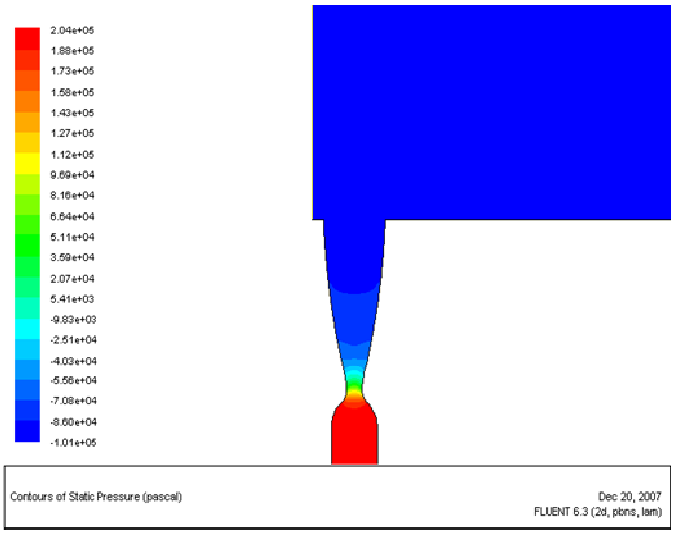

60,000m